THE UNIVERSITY OF MICHIGAN

INDUSTRY PROGRAM OF THE COLLEGE OF ENGINEERING

DIRECTIONAL CORRELATION OF GAMMA RAYS IN GERMANIUM 72 AND DYSPROSIUM 160

Robert G. Arns

A dissertation submitted in partial fulfillment
of the requirements for the degree of
Doctor of Philosophy in the
University of Michigan
1959

November, 1959

IP-400

Doctoral Committee:

Professor Marcellus L. Wiedenbeck, Chairman
Assistant Professor Paul R. Chagnon
Professor David M. Dennison
Professor Wilfred Kaplan
Assistant Professor Robert R. Lewis, Jr.

ACKNOWLEDGEMENTS

The author wishes to express his sincere appreciation to:

Professor M. L. Wiedenbeck for his kind assistance and guidance throughout the course of this work.

Raymond E. Sund for his help in recording the data and many illuminating discussions.

Dr. Emerson G. Funk, Jr. and Dr. Robert W. Lide for many helpful discussions.

The Graduate School and the Department of Physics for making available to him the Dow Chemical Company Fellowship and the Barbara Backus and Ed. H. Jewett Fellowship.

The College of Engineering Industry Program for reproducing this thesis.

The author also wishes to express his appreciation to the Office of Naval Research and the United States Atomic Energy Commission for partial support of this work.

TABLE OF CONTENTS

TABLE OF CONTENTS (CONT'D)

LIST OF TABLES

LIST OF FIGURES

LIST OF FIGURES (CONT'D)

CHAPTER I

INTRODUCTION

Angular Correlation

The energy levels of nuclei can be characterized by properties such as angular momentum (spin), parity, energy, lifetime, electric quadrupole moment, and magnetic moment. One of the important recent tasks of low-energy nuclear physics has been to determine these properties and to relate them to specific nuclear models. Often the nuclear model will suggest further properties which influence the level structure and the relative intensity and angular momentum of the emitted radiation. Angular correlation of successive nuclear radiations has proved a useful tool in determining the spin and parities of nuclear energy levels as well as the angular momentum of the radiation. The study of angular correlations under the influence of controlled extranuclear fields has also revealed important information about the electric and magnetic properties of the nucleus. All of this information has been extremely valuable in testing the predictions of nuclear models and the extent of their validity.

The probability of emission of a particle or quantum from a radioactive nucleus depends in general on the angle between the nuclear spin and the direction of emission. A completely isotropic distribution of radiation is observed, however, as long as the nuclei are randomly oriented. Under certain conditions external fields can be used to bring about a preferred orientation of nuclei. Similarly, if a nucleus emits two radiations in rapid succession (i.e., before collisions or local fields can change its orientation) observation of the first radiation

in a given direction will choose an ensemble of nuclei with an anisotropic distribution of spin orientations. Observation of the direction of the second radiation will then, in general, show an angular correlation with respect to the direction of the first radiation.

An angular correlation experiment consists in measuring the coincidence rate between successive radiations as a function of the angle between their directions of emission. Many types of angular correlation measurements have been carried out. Gamma-gamma, beta-gamma, alpha-gamma, and conversion electron-gamma angular correlations have become routine tools in nuclear spectroscopy. In the case of the gamma-gamma angular correlation it has become customary to use the term directional correlation to describe an experiment in which the coincidence rate is observed only as a function of the angle between detectors. An experiment of this type can yield information about the spins of the nuclear levels and the multipole order of the gamma rays. A polarization-directional correlation experiment, on the other hand, also observes the polarization of one or both of the gamma rays and can yield the parities of the nuclear levels.

The first theoretical calculations of a gamma-gamma directional correlation involving a pure-multipole cascade was carried out by Hamilton[1] in 1940. Early attempts to verify his results failed as a result of inadequate experimental techniques. In 1947, Brady and Deutsch[2] carried out the first successful gamma-gamma directional correlation experiments using Geiger counters as detectors. The introduction of the scintillation counter as an angular correlation detector in 1948[3] contributed significantly to the rapid development of the art since that time.

The present investigation is concerned with the gamma-gamma directional correlation experiment and its application in studying the decay of two radioactive nuclei. A method of analyzing the gamma-gamma directional correlation involving multipole mixtures is presented. Geometrical corrections are discussed in detail. The gamma rays in Ge^{72} and Dy^{160} following the beta decay of Ga^{72} and Tb^{160} have been studied and spins have been assigned to several of the levels. The multipole order of the gamma transitions was determined whenever possible. These results and the level structure have been discussed in terms of the unified model.

Elementary Theory of Gamma-Gamma Directional Correlation

A number of authors have studied the theory of angular correlation and have used various methods.[1,4-12] The approach which will be presented here is a simplified theory of the gamma-gamma directional correlation which, although it is limited in application, provides some physical insight into the problem.[13]

Consider a single gamma transition of angular momentum $\vec{L}$ between two nuclear states. Let L_z be the projection of $\vec{L}$ on the axis of quantization (z-axis). The gamma ray is then characterized by the multipolarity L and the magnetic quantum number M where $\vec{L}^2 = \hbar^2 L(L+1)$ and $L_z = M\hbar$. Assume that the transition is between specific magnetic substates characterized by the spin j' and j and the magnetic quantum numbers m' and m where $j' - j = L$ and $m' - m = M$.

Each component between two specific magnetic substates has a characteristic directional distribution $F_L^M(\theta)$ where θ denotes the angle

between the quantization axis and the direction of emission of the gamma ray. The distribution function $F_L^M(\theta)$ is independent of the nuclear spins and can be found by calculating the Poynting vector as a function of angle for radiation of multipole order L and magnetic quantum number M. Since the individual components $m' \rightarrow m$ cannot be observed separately, the total distribution will be a sum of all the individual distribution functions in which the relative population, $P(m')$, for each substate m' is included along with the relative transition probability $G(m',m)$ for each component $m' \rightarrow m$. The total directional distribution can then be written:

$$F_L(\theta) \sim \sum_{m',m} P(m') \; G(m',m) \; F_L^M(\theta) \qquad (1)$$

The relative transition probability, $G(m',m)$ depends only on m' and m and not on specific nuclear properties. It is independent of the wave functions describing the nuclear states. It can be shown by group theoretical methods[14] that $G(m',m)$ is equal to the square of the Clebsch-Gordan coefficient for the vector addition $\vec{J}' = \vec{J} + \vec{L}$, $m' = m + M$:

$$G(m',m) = (jLmM|j'm')^2 \qquad (2)$$

The relative populations $P(m')$ depend on the energies of the various substates and on the way in which the decaying level was created.

If two gamma rays are emitted from a nucleus in quick succession, the directional correlation function $W(\theta)$ is the relative probability that γ_1 is emitted at an angle θ with respect to the direction of γ_2. Choose the direction of emission of γ_1 as the quantization axis.

Then the directional correlation of the gamma cascade is identical with $F_{L_2}(\theta)$, the total directional distribution function of γ_2. The relative populations, P(m), of the intermediate state is given by the sum of all transitions $m_1 \rightarrow m$ leading into the state m. If all the m_1 states are

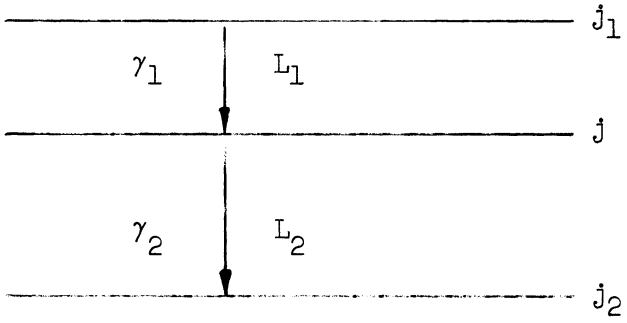

equally populated (i.e., initially the nuclei are randomly oriented), then:

$$P(m_1) \sim \sum_m G(m_1,m)\ F_{L_1}{}^{M_1}(\theta=0) \qquad (3)$$

A photon moving in a definite direction can have only the angular momentum $\pm \hbar$ along its propogation direction.[15] Hence the allowable values of M_1 are restricted to $\pm$ 1 and only the functions $F_{L_1}{}^{1}(\theta=0)$ and $F_{L_1}{}^{-1}(\theta=0)$ will appear in Equation (3).

The resultant directional correlation function is then:

$$W(\theta) = F_{L_2}(\theta) \sim \sum_{m_1,m,m_2} (jL_1m \pm 1 | j_1m_1)^2$$

$$\cdot\ F_{L_1}{}^{\pm 1}(\theta=0)(j_2L_2m_2M_2|jm)^2\ F_{L_2}{}^{M_2}(\theta) \qquad (4)$$

Since the $F_L{}^{M}(\theta)$ can be expressed in powers of $\cos^2\theta$, $W(\theta)$ becomes expressible as a series of even powers of cos θ. The evaluation of (4) for various spins and multipolarities is quite tedious for all but the

simplest cases. This difficulty was overcome in the general development of angular correlation theory. The theory was also extended to include gamma rays of mixed multipolarity, radiations other than gamma rays, and cases where the intermediate state is perturbed by extranuclear fields. It has proved more convenient to express the correlation function as a series of even-order Legendre polynomials and this convention will be adopted in what follows.

It has been assumed that the intermediate state is not perturbed by extranuclear fields, i.e., the substates of the intermediate level of the cascade are not repopulated during the lifetime of the state. The detection of the first gamma ray picks out an ensemble of nuclei with a preferred orientation in space. If strong extranuclear fields are present the nuclei may change their orientation (i.e., magnetic sublevel) before the second gamma ray is emitted. The information provided by the detection of the first gamma ray will be partially lost and the correlation will be attenuated. For states with lifetimes longer than $\sim 10^{-11}$ seconds perturbations are possible and in order to avoid an attenuation a suitable environment must be provided in which extranuclear fields are small (e.g., at a regular lattice site of a cubic crystal) or where their time average vanishes (e.g., in a dilute solution).

It is readily seen from Equation (4) that the gamma-gamma directional correlation function depends on five parameters, namely the spins of the three levels and the multipole order of the gamma transitions. Although the directional correlation experiment yields information about these parameters, additional information is always needed if a unique assignment is to be made to a sequence.

It should be noted that the directional correlation does not depend on the parities of the levels involved. Classically electric and magnetic radiation of the same multipole order are related by the transformation $\vec{E} \rightarrow \vec{H}$, $\vec{H} \rightarrow -\vec{E}$. Since the Poynting vector is invariant under this transformation the directional distribution $F_L^M(\theta)$ and hence $W(\theta)$ are left unaltered. It is possible to determine the parity of the levels only if the polarization of one of the gamma rays is detected in addition to the directional correlation.

Theoretical Results for Gamma-Gamma Directional Correlations

Pure Gamma-Gamma Cascade

A gamma-gamma cascade is said to be pure if each gamma transition is of pure multipole order. For the pure sequence $j_1(L_1)j(L_2)j_2$ the directional correlation function can be written as:

$$W(\theta) = 1 + A_2P_2(\cos\theta) + \ldots + A_{k_{max}}P_{k_{max}}(\cos\theta) \qquad (5)$$

The highest term in the expansion is given by:

$$k_{max} = \text{Min}\ (2j,\ 2L_1,\ 2L_2) \qquad (6)$$

Yang[16] has shown that this selection rule follows directly from the invariance of the correlation process under rotation and inversion. It is also derivable from the properties of the expansion coefficients. In practice, terms greater than $k = 4$ have not been observed.

The expansion coefficients, A_k, can be broken up into a product of two factors each of which depends only on the parameters of one transition of the cascade. These can be written as:

$$A_k = A_k^{(1)}\ A_k^{(2)} = F_k(L_1j_1j)\ F_k(L_2j_2j) \qquad (7)$$

where the $F_k(Lj'j)$ are the F-coefficients of Biedenharn and Rose.[17] In the following discussion the notation of Ferentz and Rosenzweig[18] will be adopted in which the F-coefficient is written as $F_k(LLj'j)$. Ferentz and Rosenzweig have tabulated the F-coefficients for all reasonable combinations of spins and multipole order.

Mixed Gamma-Gamma Cascade

The directional correlation for a cascade in which one of the gamma rays is mixed, i.e., must be described by more than one value of L, was first treated by Ling and Falkoff.[7]

Assume that the first step of a cascade consists of a mixture of L_1 and $L_1' > L_1$, with a mixing ratio δ. δ is the ratio of the reduced matrix elements:

$$\delta = (j||L_1'||j_1)/(j||L_1||j_1) \tag{8}$$

The ratio of the total (i.e., angle-integrated) intensity of the L_1' pole to that of the L_1 pole is then equal to δ^2.

The directional correlation for the cascade $j_1(L_1L_1')j(L_2)j_2$ can be written as:

$$W(\theta) = W_I + \delta^2 W_{II} + 2\delta W_{III} \tag{9}$$

W_I and W_{II} are the correlation functions for the pure cascades $j_1(L_1)j(L_2)j_2$ and $j_1(L_1')j(L_2)j_2$ respectively. W_{III} is the contribution due to the interference between L_1 and L_1' and is given by:

$$W_{III} = \sum_{k\neq 0} A_k^{III} P_k(\cos\theta) \tag{10}$$

in which:

$$A_k^{III} = F_k(L_1 L_1' j_1 j)\ F_k(L_2 L_2 j_2 j) \ . \qquad (11)$$

The coefficients $F_k(L\ L'j'j)$ and the analysis of experimental data in the presence of mixtures will be discussed in the following chapter for cases in which $L' = L + 1$.

CHAPTER II

ANALYSIS OF GAMMA-GAMMA DIRECTIONAL CORRELATIONS INVOLVING MULTIPOLE MIXTURES

With the application of angular correlation techniques to more complex decay schemes, gamma rays which are not of pure multipole order have come to be expected. The interpretation of angular correlation data becomes more complex in these cases. Various methods have been suggested to facilitate the analysis when one transition is pure and the other mixed.[19,20] The present graphical method of analysis has been extended to include the case in which neither gamma ray is pure.

Mixed Multipolarity in Gamma-Gamma Directional Correlation

Denote j_1, j, and j_2 as the initial, intermediate, and final momenta of a cascade in the gamma decay of a nucleus. Let the transition between j_1 and j be a mixture of 2^{L_1} and 2^{L_1+1} poles. Similarly describe the second transition as a mixture of 2^{L_2} and 2^{L_2+1} poles. The theoretical angular correlation function will then be of the form:

$$W(\theta) = \sum_{k \text{ even}} \alpha_k^{(1)} \alpha_k^{(2)} P_k(\cos\theta) \qquad (1)$$

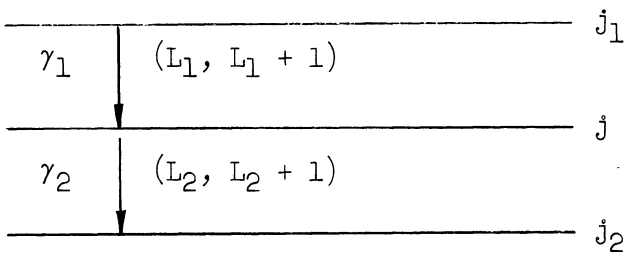

in which the constant $\alpha_k^{(\nu)}$ for the ν-th transition is dependent only upon the spins and multipolarities associated with that transition. The $\alpha_k^{(\nu)}$ are of the form:

$$\alpha_k^{(\nu)} = F_k(L_\nu, L_\nu, j_\nu, j) + 2\delta_\nu F_k(L_\nu, L_\nu+1, j_\nu, j) + \delta^2 F_k(L_\nu+1, L_\nu+1, j_\nu, j) \quad (2)$$

The summation over k in (1) runs from zero to the least of $2j$, $2(L_1+1)$, or $2(L_2+1)$. The $F_k(L, L', j', j)$ are the F-coefficients as defined and tabulated by Ferentz and Rosenzweig.[18] These are related to the definition of Biedenharn and Rose[17] as follows:

$$F_k(L\ j'\ j) = F_k(L, L, j', j)$$

$$(-1)^{j'-j-1}[(2L+1)(2L'+1)(2j+1)]^{1/2} G_k(LL'j'j) = F_k(L,L',j',j) \quad (3)$$

δ^2 is the ratio of the intensity of the $L_\nu+1$ radiation to the L_ν radiation in the ν-th transition of the cascade.

The least squares fit of experimental data in an angular correlation experiment[21] is ordinarily made to the function:

$$W'(\theta) = \alpha_o + \alpha_2 P_2 (\cos\theta) + \alpha_4 P_4 (\cos\theta) \quad (4)$$

Upon normalization this takes the form:

$$W(\theta) = 1 + B_2 A_2 P_2(\cos\theta) + B_4 A_4 P_4 (\cos\theta) \quad (5)$$

The B_k are attenuation factors depending upon the geometry of the experiment, especially detector solid angle, and:

$$A_k = (\alpha_k^{(1)}/\alpha_o^{(1)})(\alpha_k^{(2)}/\alpha_o^{(2)}) \quad (6)$$

Due to the properties of the F-coefficient for k = 0, viz.

$$F_o(L,L,j',j) = 1 \tag{7}$$

$$F_o(L,L+1,j',j) = 0 \tag{8}$$

Equation (6) becomes:

$$A_k = A_k^{(1)} A_k^{(2)} = [\alpha_k^{(1)}/(1+\delta_1^2)][\alpha_k^{(2)}/(1+\delta_2^2)] \tag{9}$$

If Q_ν is defined as the fraction of the $L_\nu+1$ multipole in the ν-th (mixed) transition, Q_ν then bears the following relation to δ_ν:

$$Q_\nu = \delta_\nu^2/(1+\delta_\nu^2) \tag{10}$$

Then $1 - Q_\nu$ is the fraction of the L_ν multipole in the same transition and the $A_k^{(\nu)}$ become:

$$A_k^{(\nu)} = a_k^{(\nu)}(1-Q_\nu) + b_k^{(\nu)}[Q_\nu(1-Q_\nu)]^{1/2} + c_k^{(\nu)}Q_\nu \tag{11}$$

where,

$$\begin{aligned} a_k^{(\nu)} &= F_k(L_\nu, L_\nu, j_\nu, j) \\ b_k^{(\nu)} &= 2F_k(L_\nu, L_\nu + 1, j_\nu, j) \\ c_k^{(\nu)} &= F_k(L_\nu + 1, L_\nu + 1, j_\nu, j) \end{aligned} \tag{12}$$

Cascades with Dipole-Quadrupole Mixtures in One Transition

Equation (6) takes on an especially simple form if one transition is a mixture of dipole and quadrupole radiation and the other is of pure multipole order. If, for example, the mixture is in the first transition:

$$A_2 = A_2^{(1)} A_2^{(2)} = \{a_2^{(1)}(1-Q_1) + b_2^{(1)}[Q_1(1-Q_1)]^{1/2} + c_2^{(1)}Q_1\}\, a_2^{(2)} \tag{13}$$

$$A_4 = A_4^{(1)} A_4^{(2)} = c_4^{(1)} Q_1\, a_4^{(2)} \tag{14}$$

A plot of $A_2^{(1)}$ vs. Q_1 from Equation (13) is an ellipse. Equation (14) is a straight line in the variables $A_4^{(1)}$ and Q_1. Single transition mixture curves of this type have been tabulated for all transitions involving integer spins up to 6 and half-integer spins up to 11/2.[22] The least squares fit will yield values of $A_2^{(exp)} \pm \sigma_2$ and $A_4^{(exp)} \pm \sigma_4$. The σ_k's are the mean square errors defined by Rose, Equation (30).[21] In order to determine the quadrupole content of the mixed transition it becomes convenient to divide the $A_2^{(exp)} \pm \sigma_2$ and $A_4^{(exp)} \pm \sigma_4$ by the corresponding $a_2^{(\nu)}$ and $a_4^{(\nu)}$ from the unmixed transition. The resultant numbers are then to be compared with the single transition mixture curves described above in order to find the range of Q consistent with the experiment. A number of examples of this method of analysis are included in the experimental section of this thesis.

Cascades with Mixtures in Both Transitions

If both steps of a cascade are mixtures of dipole and quadrupole radiation, both $A_2^{(1)}$ and $A_2^{(2)}$ have the form of Equation (11). A_4 reduces to:

$$A_4 = A_4^{(1)}A_4^{(2)} = (c_4^{(1)}Q_1)(c_4^{(2)}Q_2) \tag{15}$$

The set of values of the $A_k^{(\nu)}$ satisfying:

$$A_k^{(1)}A_k^{(2)} = A_k^{(exp)} \pm \sigma_k \tag{16}$$

can be calculated. These can be plotted as an area between equilateral hyperbolae. Various single transition mixture curves can be placed with scales to coincide with the $A_k^{(\nu)}$ axes of the experimental graph, i.e., graph of Equation (16). Then a range of Q_1 consistent with the first

transition will correspond to a range of values of Q_2 for the second transition required by the experimental graph and vice versa. Additional information is always needed in order to obtain unique assignments from angular correlations involving double mixtures. Often limits can be placed on the mixture in one transition from internal conversion data or from other angular correlation measurements. This information can then be incorporated into the graphical analysis.

Application of this method to a typical doubly mixed sequence is shown in Figure 1. The experimental coefficient, $A_2 = -0.1614 \pm 0.0015$, was measured by Klema for the 208 kev - 113 kev cascade in Hf^{177}.[23] Auxiliary information is available in the form of K- conversion coefficients measured by McGowan et al.[24], and Marmier and Boehm.[25] These are shown in Table I. The ground state spin is known to be 7/2.[26] The 113 kev level has been reached by coulomb excitation and a spin of 9/2 was assigned.[27] Thus (as has been assumed in Figure 1) the 113 kev transition is of the form 9/2 (D,Q) 7/2 with known mixing ratio. If the experimental K- conversion coefficients of McGowan are interpreted using Sliv's[28] calculated K-conversion coefficients, the 208 kev transition is found to be an E1 + M2 mixture with $Q \leq 0.009$, and the 113 kev transition is an M1 + E2 mixture with $.896 \leq Q_2 \leq .994$. These are in agreement with conversion ratio measurements by Wiedling.[29] Figure 1 illustrates a 9/2 (D,Q) 9/2 (D,Q) 7/2 cascade. It is seen that the experimental A_2 coefficient is consistent with a 9/2 (D,Q) 9/2 assignment for the 208 kev gamma with any value of Q_1. However, the absence of an A_4 coefficient from the angular correlation requires a small value for Q_1. The angular correlation is then clearly consistent with the conversion data. Both

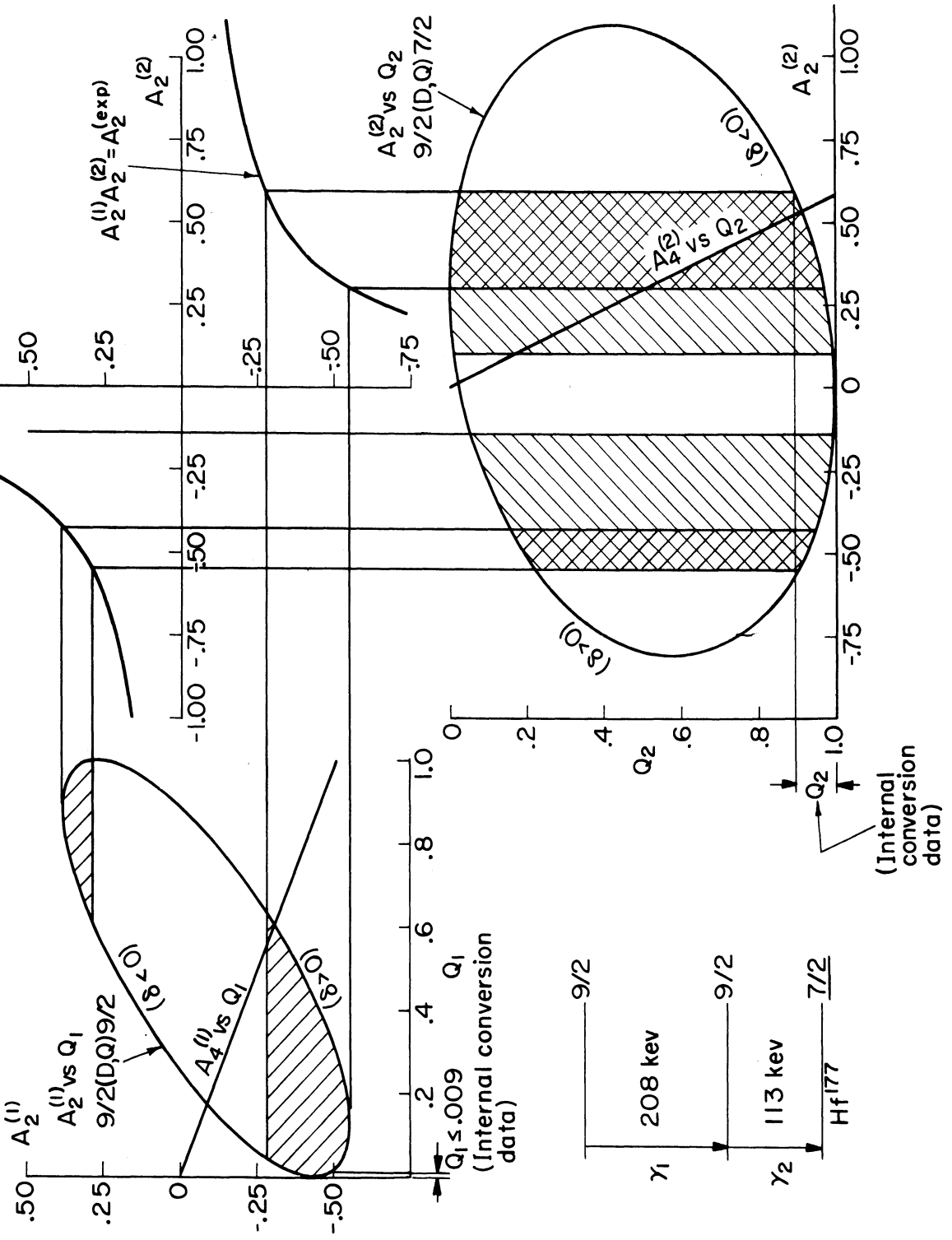

Figure 1. Analysis of Angular Correlation Data for a 9/2 (D,Q) 9/2 (D,Q) 7/2 sequence in Hf^{177}.

TABLE I

MEASURED K-CONVERSION COEFFICIENTS FOR THE 208 KEV AND 113 KEV GAMMA RAYS IN Hf^{177}

E_γ	McGowan et al.	Marmier and Boehm
208 kev	0.042 ± 0.015	0.044
113 kev	0.81 ± 0.08	0.75

the angular correlation and the conversion data will also fit a 7/2 (D,Q) 9/2 (D,Q) 7/2 sequence, but this possibility has been eliminated by Wiedling on the basis of other data.[29] Thus the angular correlation confirms the spin assignment of 9/2 for the 321 kev level in Hf^{177} and the predominantly dipole character of the 208 kev transition.

Notation

The following pages contain a number of useful single transition mixture curves. Wherever possible these have been arranged according to whether the spin of the intermediate state is larger than, equal to, or smaller than that of the other state of the transition. This arrangement shows a systematic trend in the shapes of the curves which is useful in the qualitative interpretation of experimental data.

Each curve is identified by the spins of the two states involved in the transition. They are listed in the form: j (D, Q) j', where in all cases j is the spin of the intermediate state. j' is the spin of the

initial or final state of the cascade depending on whether the graph is used to describe the first or second transition.

A list of the coefficients $a_2^{(\nu)}$, $b_2^{(\nu)}$, $c_2^{(\nu)}$ and $c_4^{(\nu)}$ used in computing the graphs is appended in Table II.

Often it is desirable to know the mixing in terms of δ, the mixing parameter. In each case where $b_2^{(\nu)}$ [as defined in (12) and listed in Table II] is positive, the upper portion of the ellipse corresponds to δ positive. If $b_2^{(\nu)}$ is negative, the opposite is true.

Table II

COEFFICIENTS $a_2^{(\nu)}$, $b_2^{(\nu)}$, $c_2^{(\nu)}$ AND $c_4^{(\nu)}$ USED IN COMPUTATION OF THE SINGLE TRANSITION MIXTURE CURVES

j	j'	$a_2^{(\nu)}$	$b_2^{(\nu)}$	$c_2^{(\nu)}$	$c_4^{(\nu)}$
1	1	-0.3536	-2.1213	-0.3536	0
1	2	+0.0707	+0.9487	+0.3536	0
2	1	+0.4183	-1.8708	-0.2988	+0.7127
2	2	-0.4183	-1.2247	+0.1281	-0.3054
2	3	+0.1195	+1.3093	+0.3415	+0.0764
3	2	+0.3464	-1.8974	-0.1237	+0.6701
3	3	-0.4330	-0.8660	+0.2268	-0.4467
3	4	+0.1443	+1.4434	+0.3093	+0.1489
4	3	+0.3134	-1.8804	-0.0448	+0.6088
4	4	-0.4388	-0.6708	+0.2646	-0.4981
4	5	+0.1595	+1.5136	+0.2849	+0.1937
5	4	+0.2944	-1.8619	0.0000	+0.5666
5	5	-0.4416	-0.5477	+0.2831	-0.5230
5	6	+0.1698	+1.5566	+0.2669	+0.2241
6	5	+0.2820	-1.8464	+0.0288	+0.5370
6	6	-0.4432	-0.4629	+0.2936	-0.5370
3/2	1/2	+0.5000	-1.7321	-0.5000	0
3/2	3/2	-0.4000	-1.5492	0.0000	0
3/2	5/2	+0.1000	+1.1832	+0.3571	0
5/2	3/2	+0.3742	-1.8974	-0.1909	+0.7054
5/2	5/2	-0.4276	-1.0142	+0.1909	-0.3968
5/2	7/2	+0.1336	+1.3887	+0.3245	+0.1176
7/2	5/2	+0.3273	-1.8898	-0.0779	+0.6367
7/2	7/2	-0.4364	-0.7559	+0.2494	-0.4775
7/2	9/2	+0.1528	+1.4832	+0.2962	+0.1737
9/2	7/2	+0.3028	-1.8708	-0.0197	+0.5857
9/2	9/2	-0.4404	-0.6030	+0.2752	-0.5125
9/2	11/2	+0.1651	+1.5374	+0.2752	+0.2102

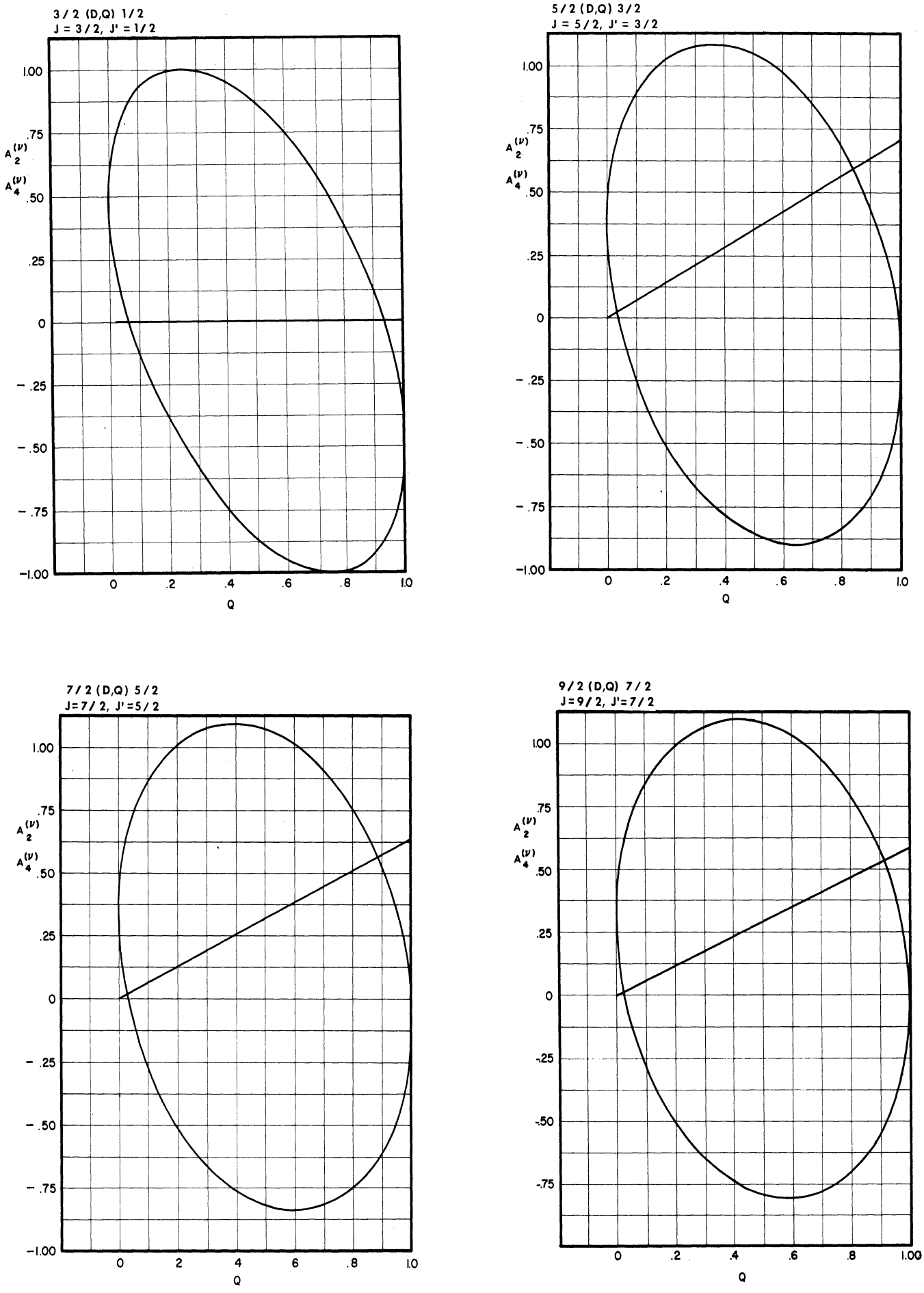

Figure 2. Single Transition Mixture Curves; 3/2 (D,Q) 1/2, 5/2 (D,Q) 3/2, 7/2 (D,Q) 5/2, 9/2 (D,Q) 7/2.

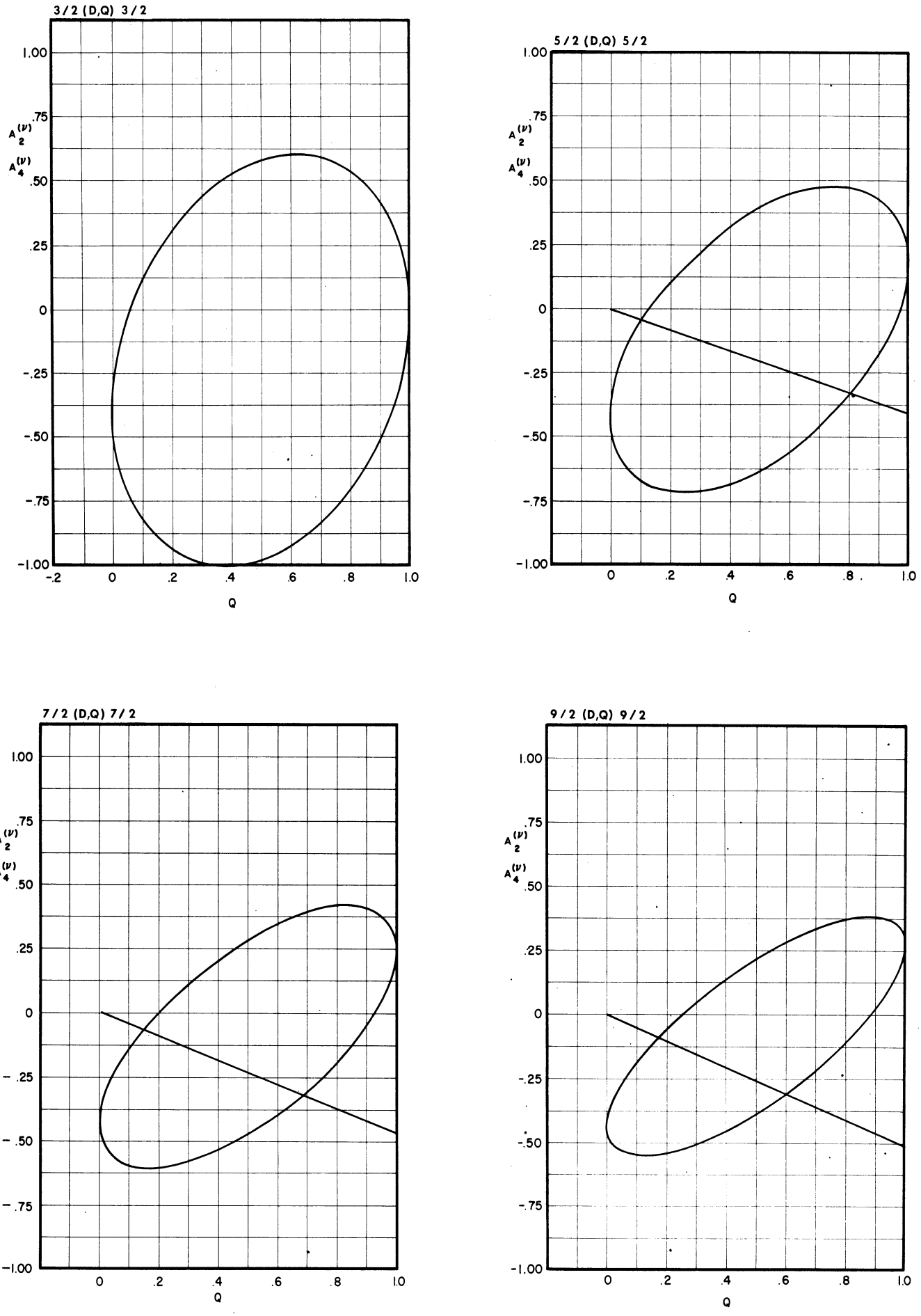

Figure 3. Single Transition Mixture Curves; 3/2 (D,Q) 3/2, 5/2 (D,Q) 5/2, 7/2 (D,Q) 7/2, 9/2 (D,Q) 9/2.

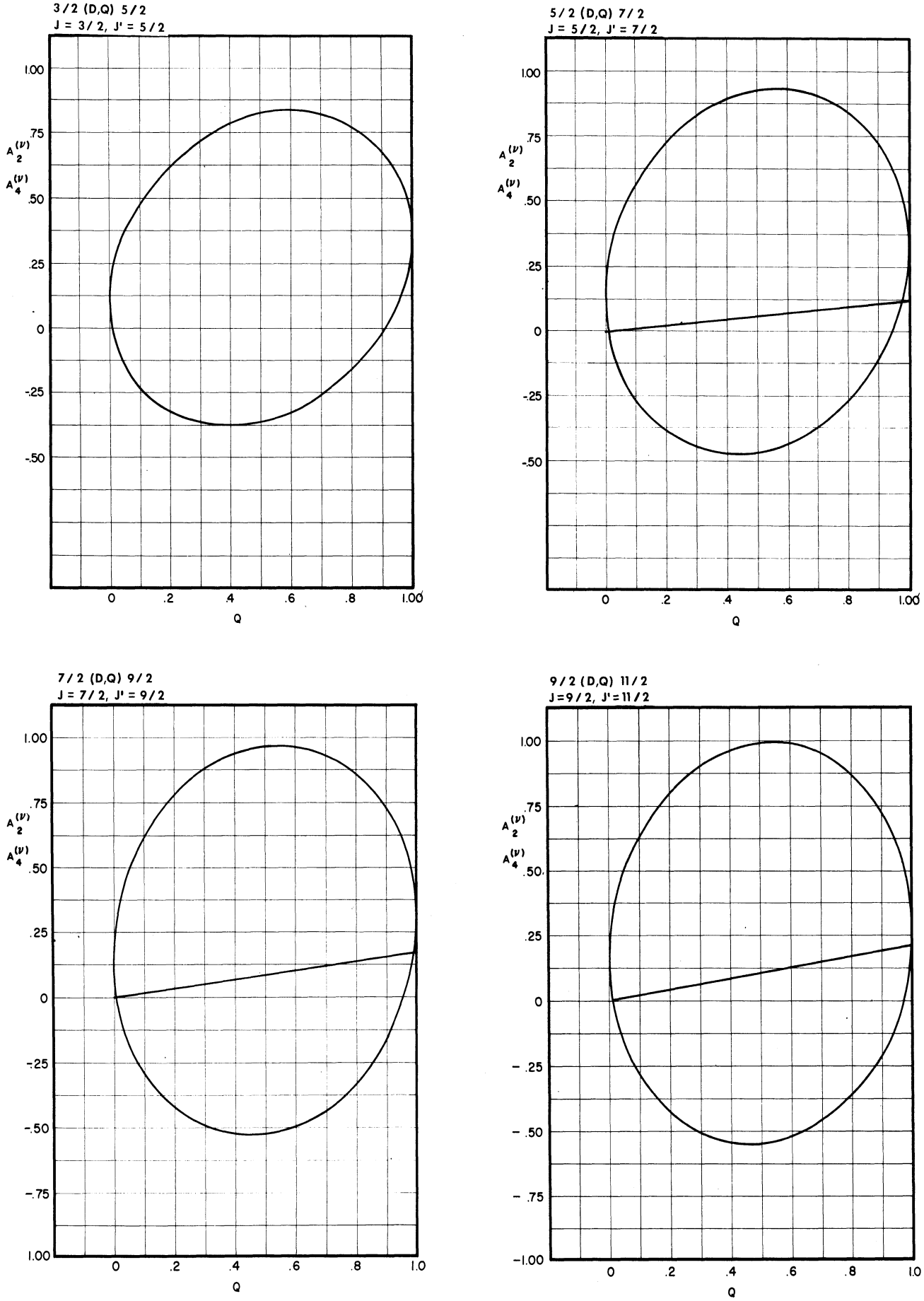

Figure 4. Single Transition Mixture Curves; 3/2 (D,Q) 5/2, 5/2 (D,Q) 7/2, 7/2 (D,Q) 9/2, 9/2 (D,Q) 11/2.

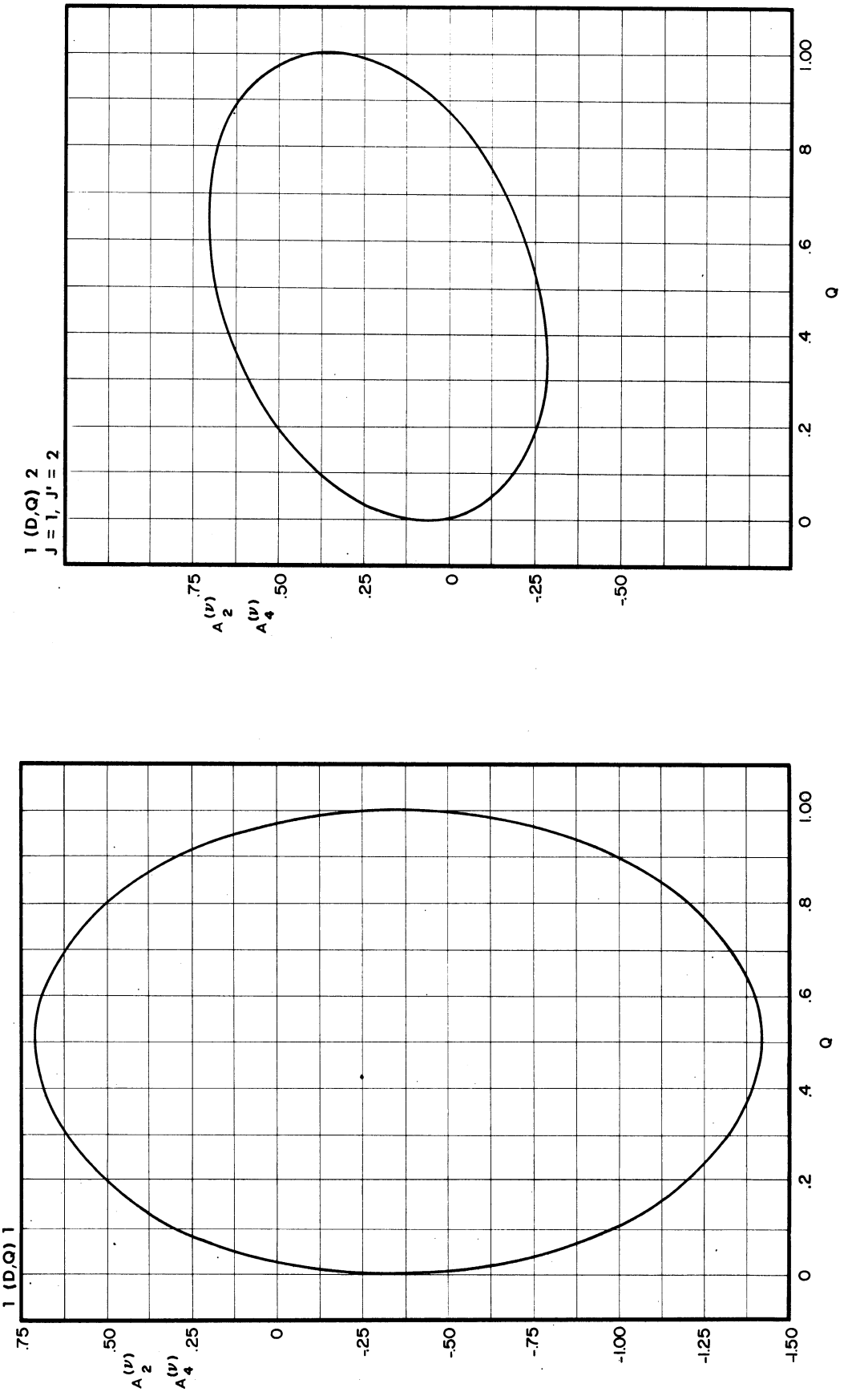

Figure 5. Single Transition Mixture Curves; 1 (D,Q) 1, 1 (D,Q) 2.

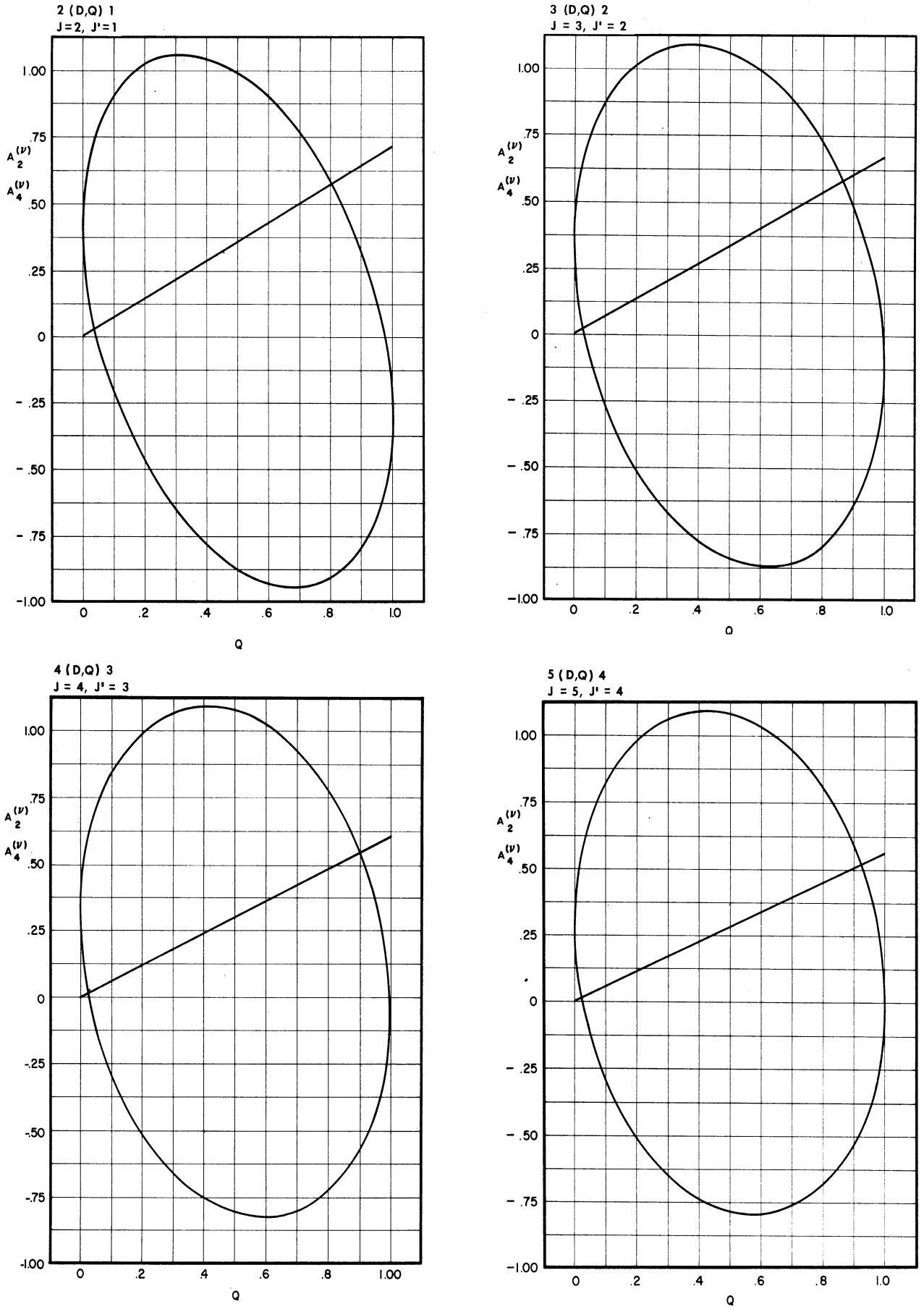

Figure 6. Single Transition Mixture Curves; 2 (D,Q) 1, 3 (D,Q) 2, 4 (D,Q) 3, 5 (D,Q) 4.

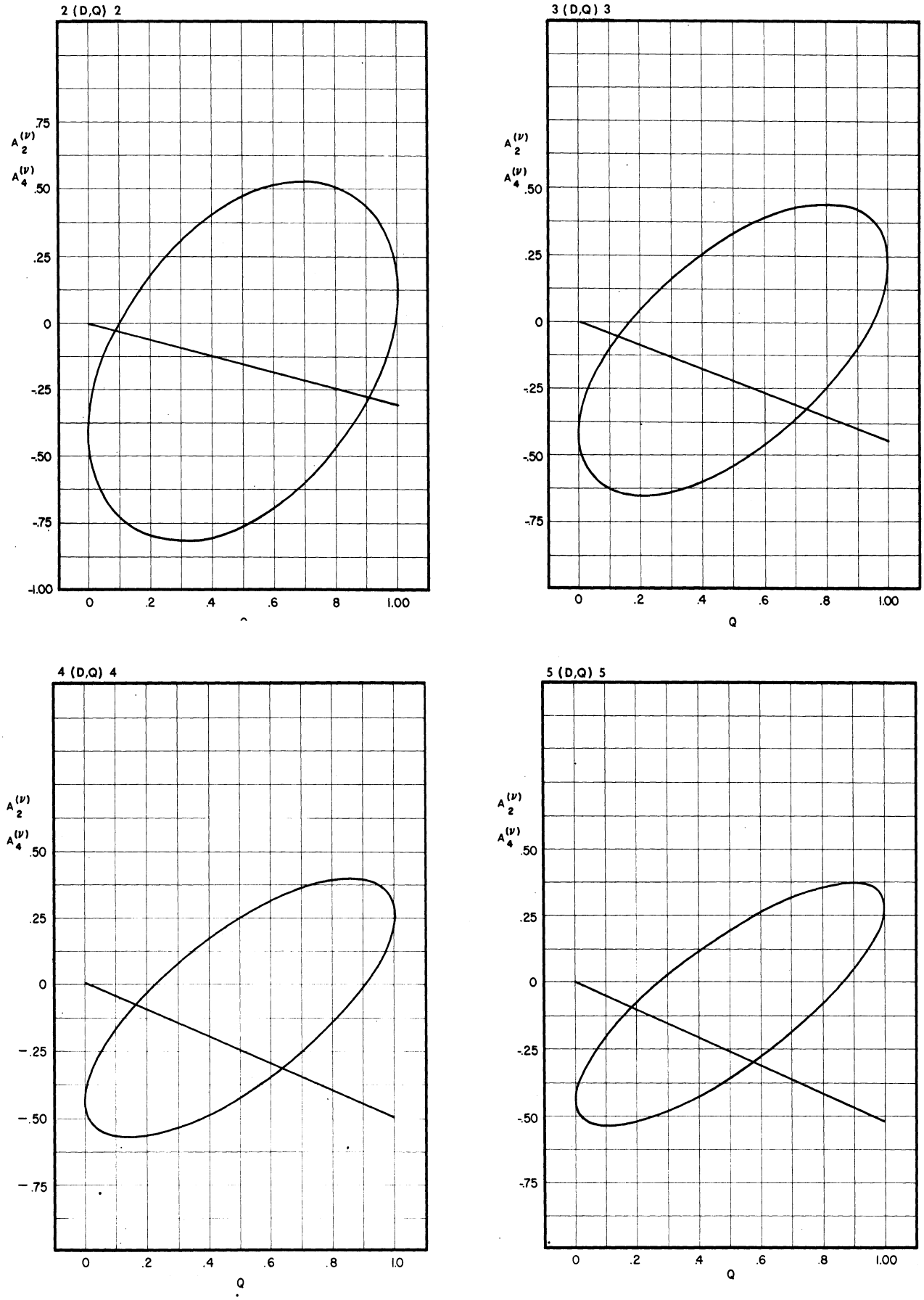

Figure 7. Single Transition Mixture Curves; 2 (D,Q) 2, 3 (D,Q) 3, 4 (D,Q) 4, 5 (D,Q) 5.

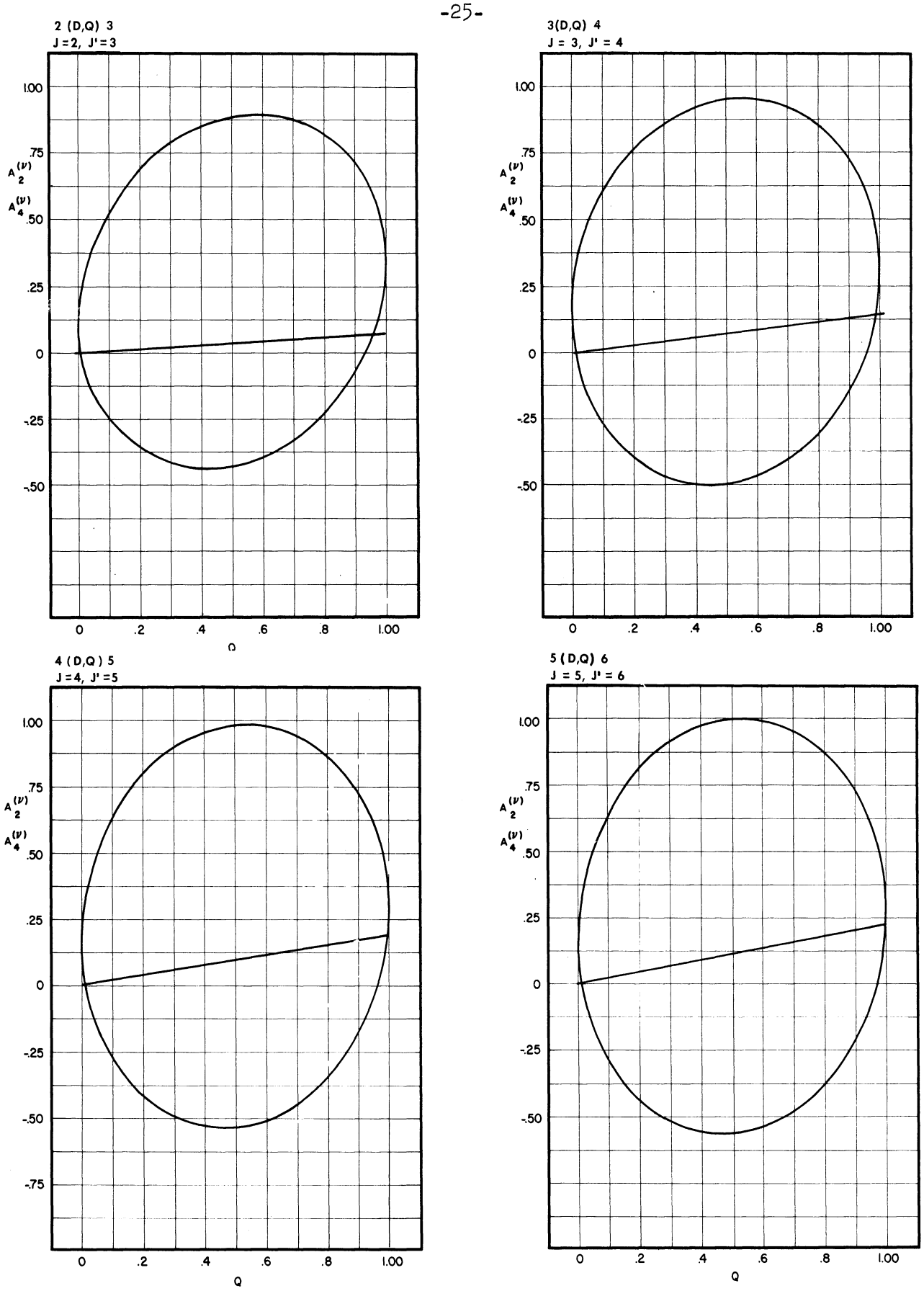

Figure 8. Single Transition Mixture Curves; 2 (D,Q) 3, 3 (D,Q) 4, 4 (D,Q) 5, 5 (D,Q) 6.

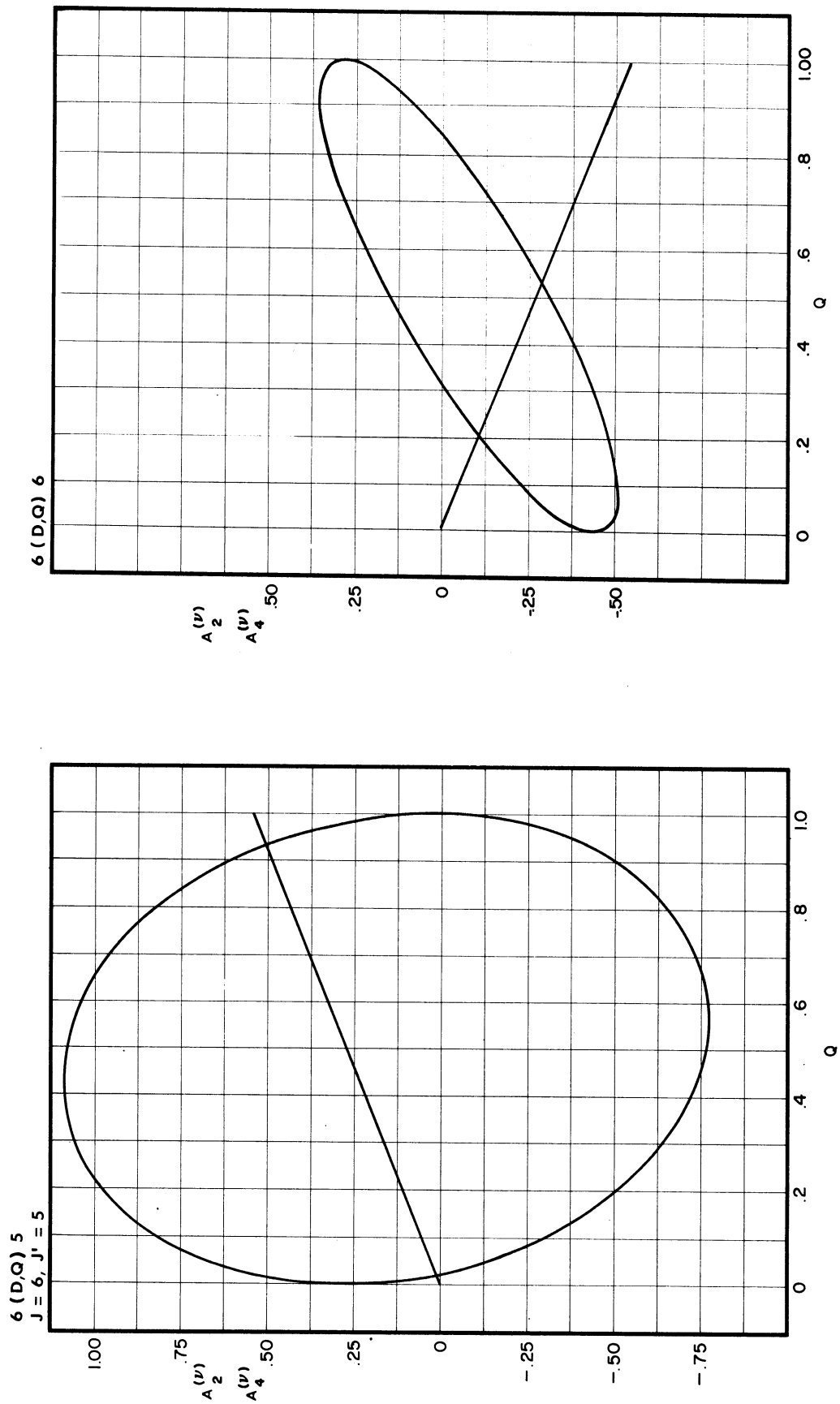

Figure 9. Single Transition Mixture Curves; 6 (D,Q) 5, 6 (D,Q) 6.

CHAPTER III

EXPERIMENTAL CONSIDERATIONS

The Coincidence Method

The directional correlation experiment consists in measuring the coincidence rate between successive radiations as a function of the angle between their directions of emission. If the decay of a nucleus involves many gamma rays it is necessary to establish the decay scheme and the relative intensities of the various cascades before a directional correlation experiment can be attempted. After the coincidence spectrum has been established, the directional correlation experiment measures the coincidence rate versus angle for a portion of this spectrum, i.e., one cascade.

Resolving Time

In addition to the real coincidences which are due to simultaneous detection of two gamma rays from the same nucleus, there will always be chance coincidences arising from simultaneous detection of two gamma rays from different nuclei. The degree of simultaneity required to record a coincidence is governed by the resolving time, τ, of the coincidence circuit. The real coincidence rate, N_R, is given by

$$N_R = N_T - N_A \tag{1}$$

where N_T is the total coincidence rate and N_A is the chance or accidental coincidence rate.

The accidental coincidence rate may be expressed as[30]

$$N_A = 2\tau N_1 N_2 \tag{2}$$

where N_1 and N_2 are the counting rates of the individual detectors. The accidental coincidence rate is determined experimentally by measuring

the coincidence rate from two independent sources, each of which can be "seen" by only one of the detectors. All of the coincidences recorded are then accidental coincidences and the observed rate can be subtracted from the total coincidence rate. This method can also be used to determine the resolving time of a coincidence circuit.

Assuming no correlation, the real coincidence rate may be expressed as:

$$N_R = N\ \sigma_1\epsilon_1\ \sigma_2\epsilon_2 \tag{3}$$

where N is the source strength (in disintegrations per unit time), σ_1 and σ_2 are the solid angles subtended by the two detectors, and ϵ_1 and ϵ_2 are the efficiencies of the detectors. The counting rate of each detector is:

$$N_i = N\ \sigma_i\epsilon_i \tag{4}$$

Inserting these in Equation (2), one obtains:

$$N_A = 2\tau\ N^2\ \sigma_1\epsilon_1\ \sigma_2\epsilon_2 \tag{5}$$

Dividing Equation (3) by Equation (5), the real to accidental coincidence ratio is obtained:

$$N_R/N_A = 1/(2\tau N) \tag{6}$$

This ratio should be kept as large as possible in order to reduce the correction to the total coincidence rate. Since N_R is proportional to the source strength, N, a lower limit on N is imposed by the minimum tolerable real coincidence rate. Thus the resolving time must be kept as small as possible if the real to accidental ratio is to be large. Unfortunately the resolving time cannot be made arbitrarily small due to the properties of the scintillator and photomultiplier tube. It can be shown that the resolving time, τ, should not be less than the

decay time of the light signal from the scintillator if energy selection is to be maintained and all real coincidence events are to be registered by the coincidence circuit. The usual scintillator employed in gamma-gamma coincidence measurements is thallium-activated sodium iodide. This has the advantage of good energy resolution but its decay constant is long (about 250 millimicroseconds). This would limit the resolving time to an abnormally large value if energy selection were maintained by the coincidence circuit.

Shorter resolving times can be utilized if the time and pulse height information are separated in parallel channels. This gives rise to the so-called "fast-slow" coincidence circuit. The "fast"coincidence circuit is then triggered by a small portion of the initial rise of each pulse. This process destroys energy selection in the "fast" circuits. The pulse height (and hence energy) information is fed through separate "slow" channels which provide energy selection. The output of each slow channel and the output of the fast coincidence circuit are then brought together in a slow coincidence circuit. The output of this circuit thus unites the time and energy information. The shortest resolving time obtainable in this way is ultimately limited by the statistical nature of emission of the first few photoelectrons from the cathode of the photomultiplier tube.[31,32]

In practice, a compromise is made between the real to accidental ratio and the time necessary to collect sufficient data. The resolving time is fixed and the source strength is adjusted until the best allowable ratio is obtained.

Coincidence Apparatus

Qualitative coincidence measurements were necessary in order to confirm the decay scheme in the case of Dy^{160}. The apparatus consisted of a fast-slow coincidence circuit and a multichannel analyzer of the "gray-wedge" type.[33,34] The detectors were 1-1/2" x 1" NaI(Tl) crystals mounted on RCA 6342 photomultiplier tubes. Figure 10 shows a block diagram of the apparatus. The fast and slow coincidence circuits were integral parts of the Beva Laboratories Model 210 Analyzer which was modified so that the fast-slow arrangement could be used. The "gray-wedge" display consists of a sweep on a cathode-ray tube for each pulse analyzed. The (vertical) position of the sweep is a linear function of pulse height, i.e., energy. A very large number of sweeps are photographed through a glass plate, known as the gray wedge, the transmission of which decreases from the beginning to the end of the sweep, i.e., from left to right. If there are many sweeps at a particular energy, the photograph will show a longer track than for a single sweep. This then corresponds to counting rate. The photograph thus displays the spectrum, i.e., rate versus energy, of pulses applied to the input.

Additional quantitative coincidence measurements were made using the single channel analyzers of the directional correlation apparatus. The details will be described in the following sections.

Directional Correlation Measurements

Collection of Data

The correlation function, $W(\theta)$, is measured by observing the coincidence rate as a function of the angle, θ, between the detectors. One detector is fixed in position while the other is free to rotate about

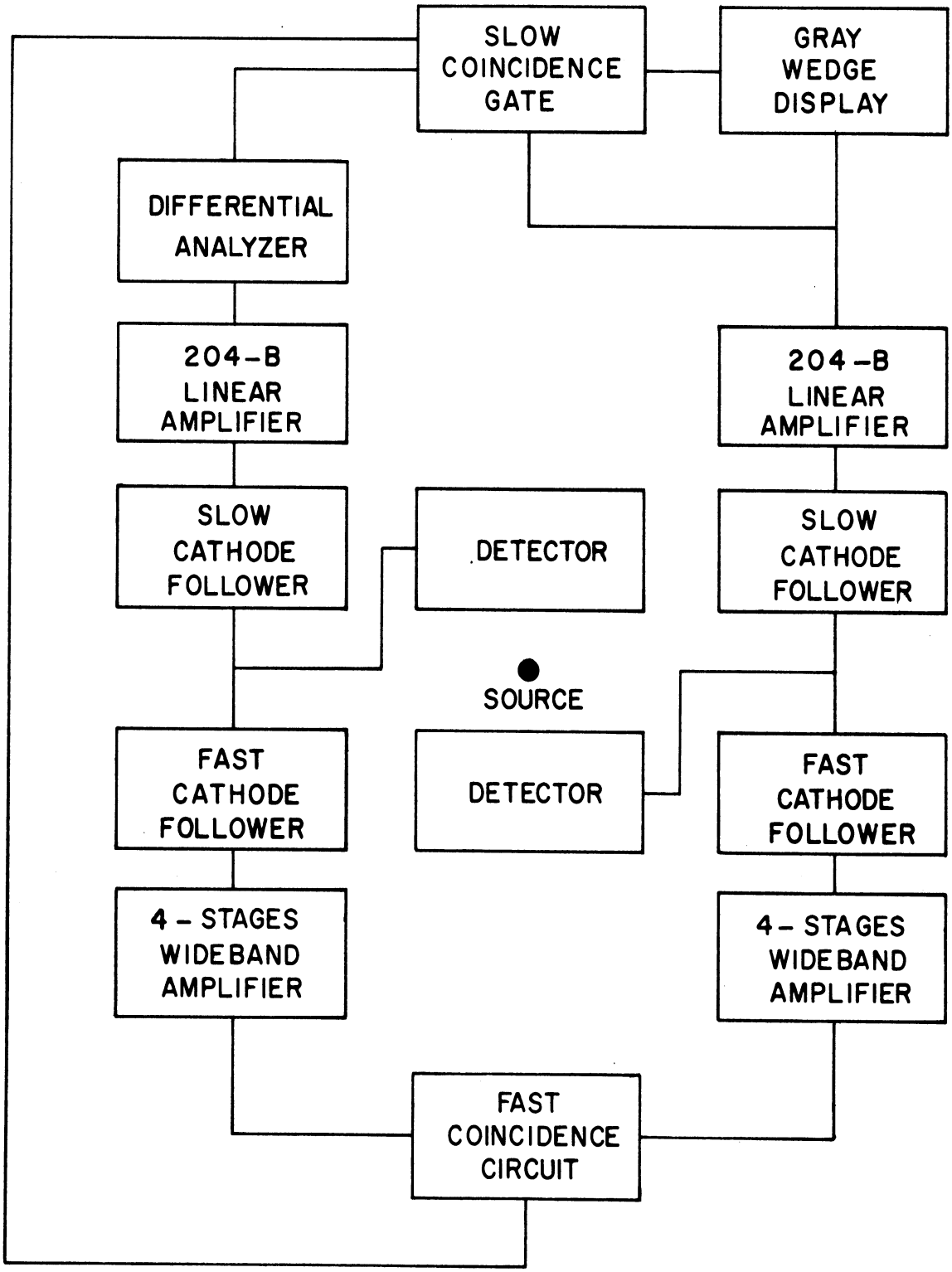

Figure 10. Qualitative Coincidence Apparatus Used in the Study of the Decay Scheme of Dy^{160}.

the centrally mounted source. The correlation function involves only the even-order Legendre polynomials and hence all of the information about the correlation can be gained by taking data in one quadrant, e.g., from $\theta = 90°$ to 180°. However, there are a number of important considerations which make it desirable to collect data in a double-quadrant sequence, i.e., from 90° to 270°. In most of the measurements presented here, the data were taken every 15° from 90° to 270°. In some of the weaker cascades data were taken only every 30°. The data from corresponding points were then added together.

Errors due to source misalignment or false assymmetries due to scattering from nearby objects are eliminated to first order by combining the corresponding points from each quadrant. The data are taken for only a short time, usually five minutes, at each point. Thus an entire run in two quadrants can be completed in at most 1-1/4 hours. This process is repeated many times until the necessary number of coincidences are collected. Errors due to decay of the source and steady drift in the apparatus are eliminated by the double-quadrant sequence provided that the half-life of the decay and the period of the drift are longer than the length of a run. In addition, any short term instabilities tend to be averaged out if a large number of runs are taken.

Source Preparation

In Chapter I it was pointed out that the correlation function can be attenuated by extranuclear fields. Often, however, the full correlation can be realized if the source is in the form of a dilute solution. Even if the interaction is very large the correlation can be

partially restored in this manner.[35,36] This is due to the continual rearrangement of the perturbing fields caused by molecular collisions. The extranuclear fields may be reoriented many times during the lifetime of the intermediate state and the net effect on the nucleus will be small. All of the sources used in the present experiments were in the form of dilute aqueous solutions.

If the source is large in volume or of high density, scattering of the gamma rays within the source may attenuate the correlation. The correction for scattering in the source is complicated and difficult to apply.[37] Additional assymmetries may arise from the anisotropy of photoelectric absorption within the source.[38] In the present experiments the sources were small and tenuous and no corrections were necessary. The source holders were machined from lucite with a cylindrical cavity for the source 0.3 cm in diameter and 1.0 cm high. The wall was .025 cm thick and the cavity was capped and supported on a thin lucite rod.

Directional Correlation Apparatus

A fast-slow coincidence spectrometer was employed in all of the directional correlation measurements. The major features of this circuit were designed by R. Scharenberg and M. Stewart.[39,40] A block diagram of the apparatus is shown in Figure 11. The individual portions of the spectrometer will be discussed in more detail in the following sections.

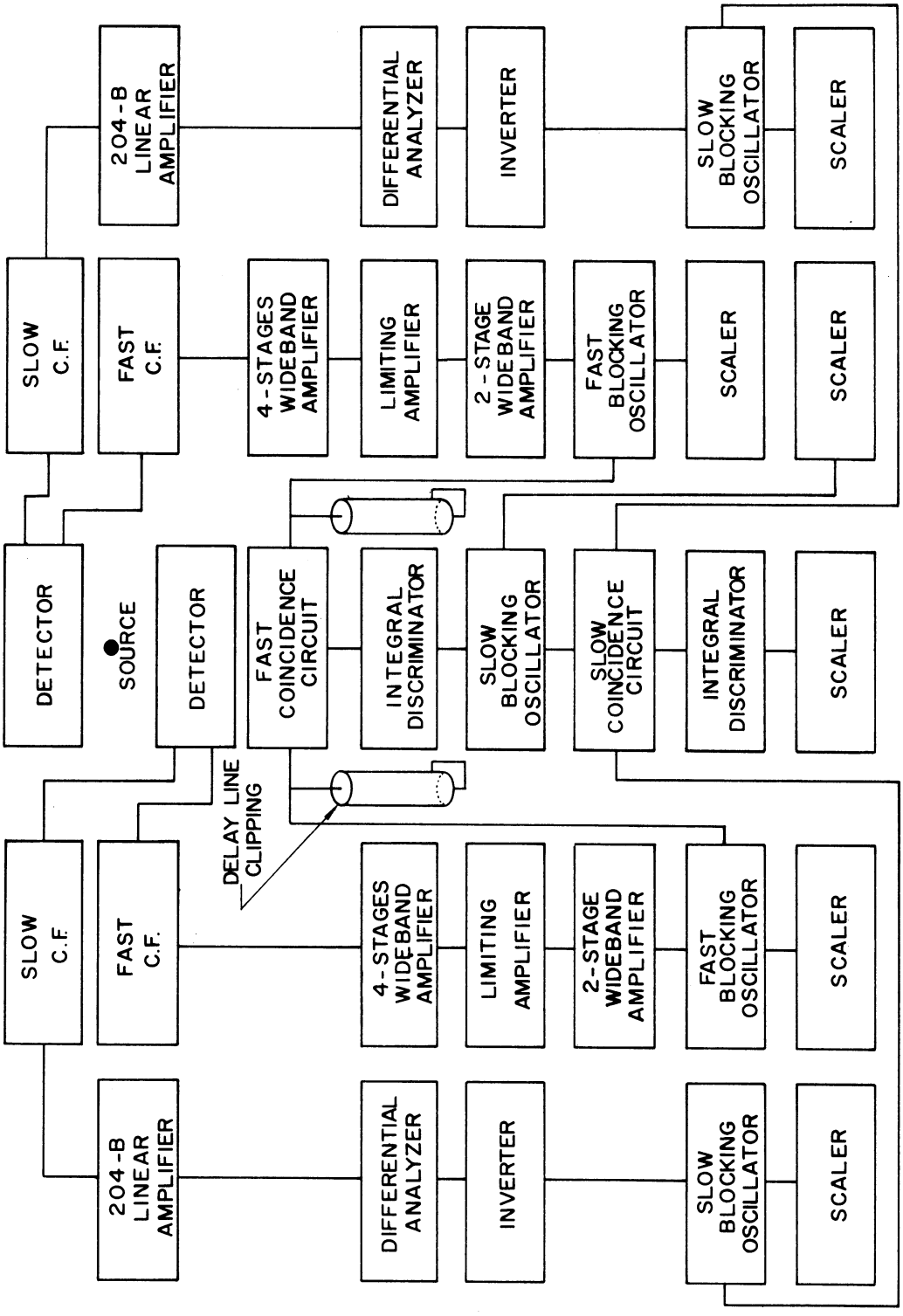

Fig. 11 Fast-Slow Coincidence Spectrometer Used in the Directional Correlation Measurements.

Detectors

The gamma ray detectors for most of the directional correlation measurements consisted of 2" x 2" NaI(Tl) crystals mounted on RCA 6342 photomultiplier tubes. The crystals were coupled to the photomultiplier tubes with Dow-Corning 200 Fluid (viscosity = 10^6 cs.). The phototubes were magnetically shielded with mu-metal and mounted within a 3" diameter iron pipe with the crystal projecting through the front cap. The resultant scintillation counters had an energy resolution of about 10% for the 0.662 Mev gamma ray of Cs^{137}.

The detector of one of the gamma rays in a weak cascade (1.88 Mev - 1.46 Mev) in Ge^{72} consisted of a 5" x 4" NaI(Tl) crystal mounted on a DuMont 6364 photomultiplier tube. The increased efficiency of this crystal made a measurement feasible in this very weak cascade.

The scintillation counters were shielded frontally with 3/16" of aluminum to prevent beta particles from entering the crystals. Lateral lead shielding was used in many of the measurements to prevent crystal to crystal scattering. Crystal to crystal scattering may occur when a gamma ray is absorbed in a crystal by the Compton effect. The scattered photon may then escape the first crystal and enter the second. If it is absorbed in the second crystal a coincidence is produced. In some cases energy selection cannot adequately eliminate these coincidences and false assymmetries can thus be introduced. In these cases it is necessary to shield the crystals from one another. The shields employed in the present measurements were hollow lead cylinders, 3/4" thick, which surrounded the sides of the crystals and extended 1" beyond the front face. These precautions also serve to eliminate errors due to scattering from surrounding objects.

Fast Coincidence Circuit

The primary factor in determining the resolving time of a coincidence circuit is the duration of the input pulses. Moreover, proper functioning demands pulses of uniform size and shape. The slow-rising and non-uniform pulses of the scintillation counter must be converted to short, fast, and uniform pulses. This is accomplished at the expense of losing all information about the amplitude of the pulse.

The negative pulse from the scintillation counter is fed from a cathode follower through 200 ohm coaxial cable to a series of transmission line amplifiers (Hewlett-Packard types 460A and 460B) each of which has a maximum gain of about eight and a bandwidth of 100 megacycles.

The highly amplified pulses are made uniform in height by a limiting amplifier. This output pulse is again amplified by a two stage wideband amplifier and used to trigger a fast blocking oscillator. The uniform and short pulse from the blocking oscillator is clipped by a shorted delay line to a width of about 18 millimicroseconds. The pulses from each detector, shaped in this way, are fed into a Garwin type coincidence circuit.[41,42] The output pulses from the coincidence circuit are selected by an integral discriminator. The resolving time for all of the present measurements was $\tau = 18$ millimicroseconds.

Energy Selection

In addition to the fast channels described above, the pulses from each detector are also fed into a parallel slow channel which has the function of providing energy selection. Initially the output pulses

are amplified without distortion by means of a 204-B linear amplifier. These pulses are then fed into a differential pulse height analyzer of the Johnstone[43] type as modified by Lu.[44] This circuit gives a uniform output pulse whenever the input pulse height is between two predetermined voltage levels. Since the pulse height is a linear function of energy, this provides a means of picking out particular energies and rejecting others.

If the nucleus being studied has many gamma ray cascades, the interpretation of a single directional correlation measurement is often complicated by interference from other cascades. The use of scintillation counters as detectors helps to overcome this difficulty. However, the presence of unresolved peaks and pulses accompanying the escape of Compton-scattered gamma rays from the crystal makes it impossible in many cases to achieve complete energy selection. In these cases it is often possible to correct the data by subtracting the interference.[45] The methods used depend upon the individual case and will be discussed separately for each cascade studied.

Slow Coincidence Circuit

Energy selected pulses from each slow channel and the output pulse of the fast coincidence circuit are brought together in a triple coincidence circuit. The function of this slow circuit is to unite the time and energy information and provide an output pulse only when all of the imposed conditions are met. The input pulses trigger blocking oscillators which provide a uniform pulse 200 millimicroseconds in duration. These are then fed into a Garwin coincidence circuit similar

to that used in the fast circuit. The resolving time is 200 millimicroseconds. The output of the triple coincidence circuit is sent to an integral discriminator where the smaller single and double pulses are rejected and the triple coincidence pulses are passed on to a scaler.

Recording

Five scalers were used to record the pulses of the blocking oscillators in each of the coincidence circuits. A sixth scaler recorded the final output of the triple coincidence circuit. Conventional binary scalers were used in all cases. The slow channel rates were often used in computing corrections to the observed triple coincidence rates.

Treatment of Data

After correcting the data of each run for the accidental coincidence rate, all of the data at a given angle were added together. A least squares fit was then made to the function

$$W'(\theta) = \alpha_0 + \alpha_2 P_2 (\cos \theta) + \alpha_4 P_4 (\cos \theta) \qquad (7)$$

according to a procedure outlined by Rose.[21] The coefficients were then normalized to the form:

$$W(\theta) = 1 + B_2 A_2 P_2 (\cos \theta) + B_4 A_4 P_4 (\cos \theta)$$

where the B_k are normalized attenuation coefficients which are introduced by the finite size of the source and detectors. These will be treated in detail in the following section. The final experimental coefficients, $A_2^{(exp)} \pm \sigma_2$ and $A_4^{(exp)} \pm \sigma_4$, were then analyzed according to the method outlined in Chapter II.

Geometrical Corrections

The expansion functions ordinarily encountered in the angular correlation of successive nuclear radiations vary slowly and smoothly as a function of angle. Because of this a successful measurement will require "good statistics" but can be made in a "poor geometry" detector system. In the case of a gamma-gamma angular correlation experiment with NaI(Tl) scintillation detectors, the maximum source strength is dependent upon the resolving time of the coincidence circuit which is inherently limited by the response of the scintillator. Often the counting rates will be further limited by detector efficiency, the branching ratio of the cascade being studied, and the necessity of using a liquid source to avoid perturbations. In order to perform the experiment in a reasonable time, it then becomes imperative to increase the solid angle subtended by the detectors and the physical size of the source without impairing the accuracy of the measurement.

The effect of a constant efficiency detector has been treated to first approximation by Walter et al.[46] for various source and detector configurations. Rose[21] and West[47] have calculated the corrections in the case of a point source of gamma radiation incident on an unshielded cylindrical scintillation detector. Lawson and Frauenfelder[48] calculated the same correction from a measured detector-efficiency function. For gamma ray energies near .5 Mev, Church and Kraushaar[49] developed a practical method of making this correction from the measured correlation for annihilation radiation. Feingold and Frankel[50] have treated theoretically the cases of axially extended sources and detectors of arbitrary shape and efficiency. Several of their equations have been

reproduced in the following application of their results to the gamma-gamma angular correlation experiment. Slight changes of notation have been made and several errors which appeared in Reference (50) have been corrected.

Arbitrary Detectors with a Point Source

The efficiency, E, of a general gamma ray detector is a function of (θ,ϕ), the coordinates specifying a point on the detector surface; and also of the coordinates which give the angle of incidence of the radiation at that point. If the efficiency of the detector is independent of incident angle, and a point source of radiation defines the center of the (θ,ϕ) coordinate system, the efficiency can be expressed as a series of the spherical harmonics, $Y_\ell^m(\theta,\phi)$. If we further assume that the two detectors, 1 and 2, are sensitive to radiations b and c, respectively, the expansions may be given as:

$$E_{b_1}(\theta_1,\phi_1) = \sum_{\ell'm'} \left(\frac{2\ell'+1}{4\pi}\right)^{1/2} b_{\ell'm'}\, Y_{\ell'}^{m'}(\theta_1,\phi_1) \qquad (1)$$

$$E_{c_2}(\theta_2,\phi_2) = \sum_{\ell''m''} \left(\frac{2\ell''+1}{4\pi}\right)^{1/2} c_{\ell''m''}\, Y_{\ell''}^{m''}(\theta_2,\phi_2) \qquad (2)$$

in which the coordinates are defined as shown in Figure 12. The experimental angular correlation,

$$W'(\theta) = \sum_\ell A'_\ell P_\ell(\cos\theta) \qquad (3)$$

can now be related to the point-point correlation,

$$W(\theta') = \sum_\ell A_\ell P_\ell(\cos\theta') \qquad (4)$$

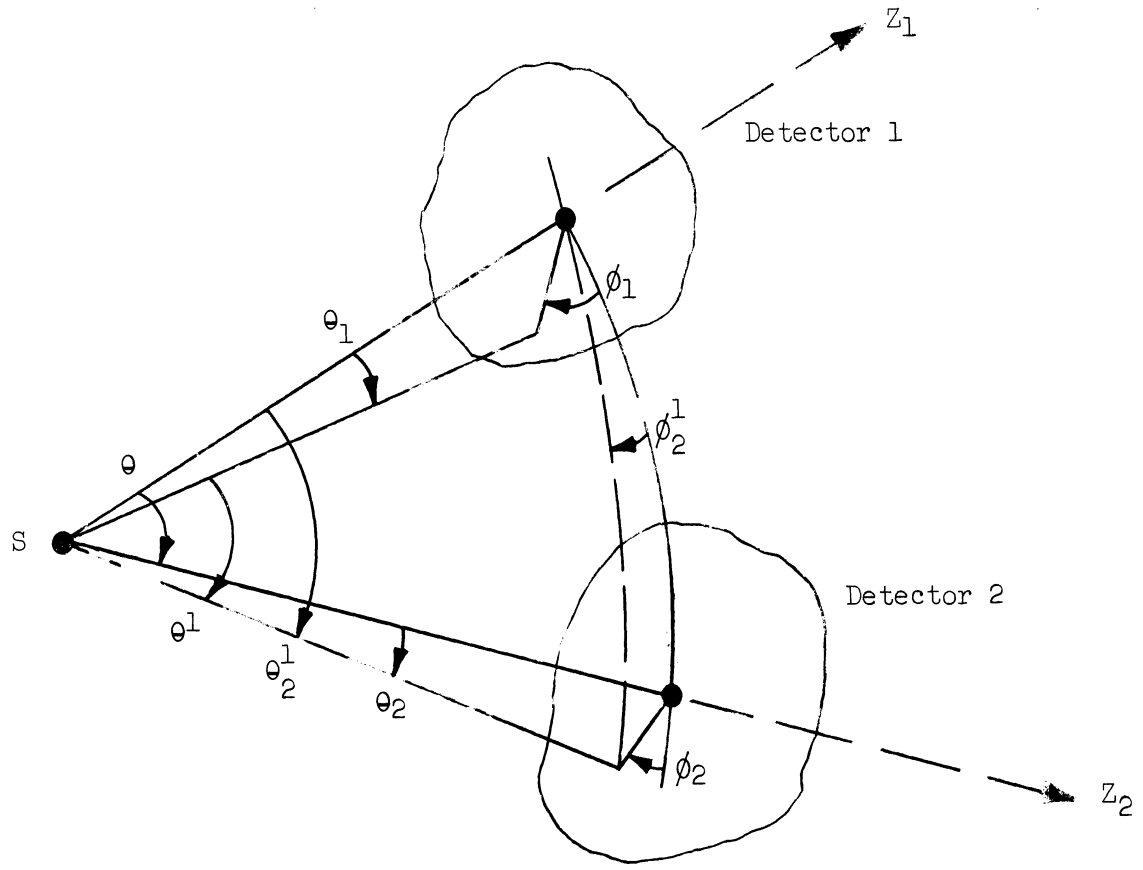

Figure 12. Geometry of the Angular Correlation Experiment.

by the relation:

$$W'(\theta) = \int \int E_{b1}(\theta_1,\phi_1)\ W(\theta')\ E_{c2}(\theta_2,\phi_2)\ d\Omega_1\ d\Omega_2 \ . \qquad (5)$$

$P_\ell\ (\cos\theta')$ may be expressed in terms of θ_1,ϕ_1 and θ_2',ϕ_2' by the addition theorem. Also $Y_{\ell''}^{m''}\ (\theta_2,\phi_2)$ may be expressed in terms of θ_2',ϕ_2' by a rotation of the coordinate system through the angle θ:

$$Y_{\ell''}^{m''}\ (\theta_2,\phi_2) = \sum_{n'} d_{n'm''}^{\ell''}\ (\theta)\ Y_{\ell''}^{n'}\ (\theta_2',\phi_2') \ . \qquad (6)$$

Now define:

$$g_{mm'}^{\ell\ell'} = \frac{2\ell+1}{4\pi} \int_{-1}^{+1} d_{mm'}^{\ell}(\theta)\ P_{\ell'}\ (\cos\theta)\ d\ (\cos\theta) \qquad (7)$$

By combining the above equations and making use of the orthonormality relation for the spherical harmonics[51], one obtains:

$$A'_\ell = \sum_{\ell' m m'} (-1)^{m+m'+\ell+\ell'} \frac{2\ell+1}{4\pi} A_{\ell'} b_{\ell' m} c_{\ell' m} g^{\ell\ell'}_{mm'} \qquad (8)$$

Feingold and Frankel[50] have tabulated the $g^{\ell\ell'}_{mm'}$ for $\ell \leq 6$ and m,m' even and have discussed the effect of various detector symmetries on the experimental angular correlation. In the special case of the ϕ-symmetric detector, the relation between the coefficients reduces to:

$$A'_\ell = A_\ell b_{\ell o} c_{\ell o} \, . \qquad (9)$$

Cylindrical Scintillation Detector With an Axial Source

An axial source is a line source centered at the origin perpendicular to the plane of the angular correlation measurement. The axial source can be looked upon as a sum of point sources displaced from the origin. Let $b_{\ell m}(\epsilon')$ be the $b_{\ell m}$ for a displacement ϵ' from the origin. For a source of length ϵ_o and density of activity $n(\epsilon')$, placed symmetrically about the origin:

$$b_{\ell m}(\epsilon_o) = \frac{\int_{-\epsilon_o/2}^{\epsilon_o/2} b_{\ell m}(\epsilon') \, n(\epsilon') \, d\epsilon'}{\int_{-\epsilon_o/2}^{\epsilon_o/2} n(\epsilon') \, d\epsilon'} \qquad (10)$$

where the $b_{\ell m}(\epsilon_o)$ contains both source and counter corrections. The $b_{\ell m}(\epsilon')$ is difficult to determine unless the detector efficiency is independent of incident angle. This requirement is not satisfied for the ordinary scintillation counter employed in gamma-gamma angular correlation

experiments. However, it will be shown below that the errors involved are not significant as long as the source extension is small compared to detector size and source-to-detector distance.

Assume that the face of the detector is circular and that $n(\epsilon')$ is constant. We may write

$$b_{\ell m} = \left(\frac{4\pi}{2\ell+1}\right)^{1/2} \int Y_\ell^m (\theta,\phi)\ \ E(\theta,\phi)\ d\Omega\ . \tag{11}$$

Upon transforming to Cartesian coordinates a the center of the detector (cf. Figure 13), Equation (11) becomes:

$$b_{\ell m}(\epsilon) = \left(\frac{4\pi}{2\ell+1}\right)^{1/2} \int_{-\infty}^{\infty} dy \int_{-\infty}^{\infty} dx\ \frac{Y_\ell^m\ (x,y-\epsilon)\ E(x,y)}{[1+x^2+(y-\epsilon)^2\ ]^{3/2}} \tag{12}$$

in which

$$x = \frac{x'}{r_o}, \quad y = \frac{y'}{r_o}, \quad \epsilon = \frac{\epsilon'}{r_o}$$

Transforming to polar coordinates on the face of the detector:

$$b_{\ell m}(\epsilon) = r_o\sqrt{\frac{4\pi}{2\ell+1}} \int_o^{\infty} r dr \int_o^{2\pi} d\omega\ \frac{Y_{\ell m}\ (r,\omega,\epsilon)\ E(r,\omega)}{[1+r^2+\epsilon^2-2\epsilon r\ \sin\ \omega]^{3/2}} \tag{13}$$

in which $r = \rho/r_o$ and $\epsilon = \epsilon'/r_o$. Equation (13) is now introduced into (10, defining $\gamma = \epsilon_o/(2r_o)$:

$$b_{\ell m}(\gamma) = \frac{1}{2\gamma}\sqrt{\frac{4\pi}{2\ell+1}} \int_{-\gamma}^{\gamma} d\epsilon \int_o^{\infty} r dr \int_o^{2\pi} d\omega\ \frac{Y_{\ell m}\ (r,\omega,\epsilon)\ E(r,\omega)}{[1+r^2+\epsilon^2-2\epsilon r\ \sin\ \omega]^{3/2}}\ . \tag{14}$$

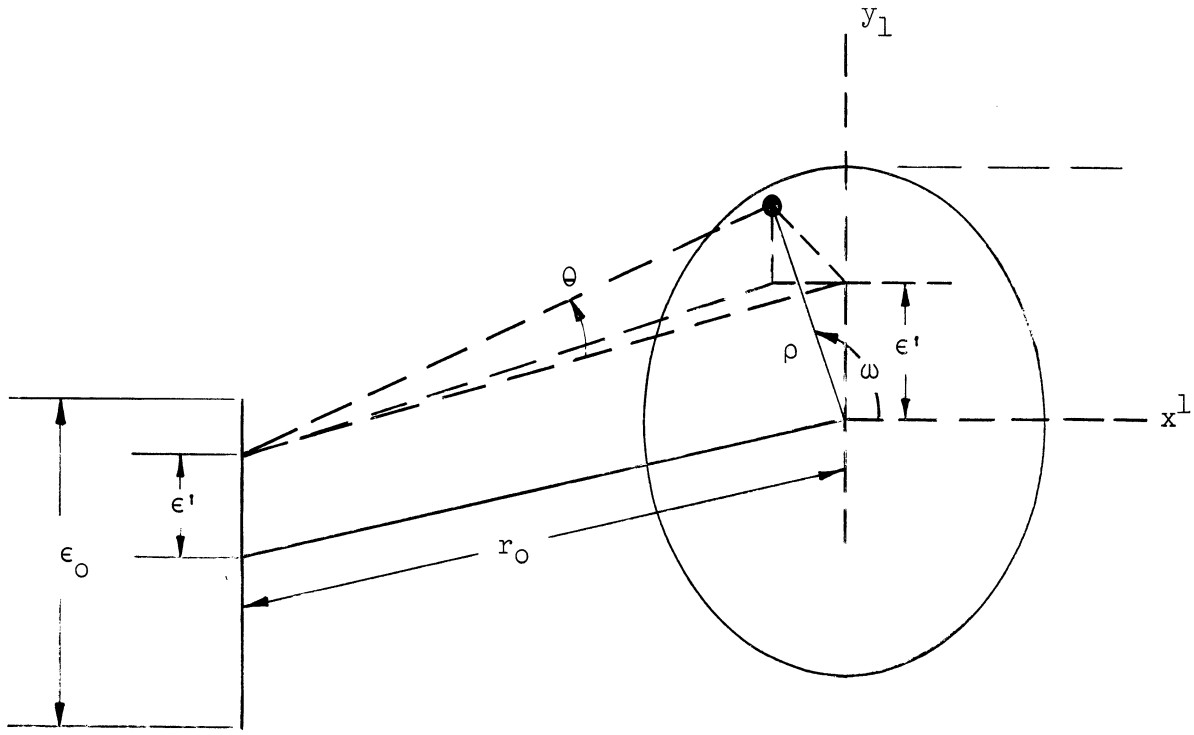

Figure 13. Geometry for a Circular Detector with an Axial Source.

If the efficiency is independent of incident angle, $E(r,\omega) = E(r)$, only the $b_{\ell o}$ terms will enter the expansion. The $Y^o_\ell(r,\omega,\epsilon) = \sqrt{(2\ell+1)/4\pi}\, P_\ell(r,\omega,\epsilon)$ can be expanded if we note that $\cos\theta = [1+r^2+\epsilon^2-2\epsilon r \sin\omega]^{1/2}$ and use the binomial expansion. Upon changing the order of the r and ϵ integrations, the $b_{\ell o}$ reduce to a series of r integrals. The coefficients b_{00}, b_{20}, and b_{40} which occur in the usual gamma-gamma angular correlation experiment are then:

$$b_{00} = 2\pi\alpha_o \left[1 - \frac{3}{2}\left(\alpha_2 + \frac{\gamma^2}{3}\right) + \frac{5}{8}\left(3\alpha_4 + 4\alpha_2\gamma^2 + \frac{3}{5}\gamma^4\right) - \ldots\right] \qquad (15)$$

$$b_{20} = 2\pi\alpha_o \left[1 - 3\left(\alpha_2 + \frac{\gamma^2}{3}\right) + \frac{15}{8}\left(3\alpha_4 + 4\alpha_2\gamma^2 + \frac{3}{5}\gamma^4\right) - \ldots\right] \qquad (16)$$

$$b_{40} = 2\pi\alpha_o \left[1 - \frac{13}{2}\left(\alpha_2 + \frac{\gamma^2}{3}\right) + \frac{25}{4}\left(3\alpha_4 + 4\alpha_2\gamma^2 + \frac{3}{5}\gamma^4\right) - \ldots\right] \qquad (17)$$

in which:

$$\alpha_o = \int_o^\infty r\, E(r)dr \qquad (18)$$

$$\alpha_2 = \frac{\int_o^\infty r^3\, E(r)dr}{\int_o^\infty r\, E(r)dr} \qquad (19)$$

$$\alpha_4 = \frac{\int_o^\infty r^5\, E(r)dr}{\int_o^\infty r\, E(r)dr} \qquad (20)$$

If $E(r)$ is measured by means of a collimated beam experiment, α_o, α_2, and α_4 can be obtained by numerical integration. The assumption that the scintillation counter is independent of incident angle introduces an error of order γ^4 and this method is therefore not valid if terms of this order contribute significantly to the $b_{\ell o}$.

Application to Typical Geometries

The efficiency functions, $E(r)$, were determined for a 2-in. by 2in. cylindrical NaI(Tl) crystal for various energies and at source to detector distances of 7.00 and 9.90 cm. The crystal was mounted on an RCA 6342 phototube and the counting rate was observed as the scintillation counter was moved through small angles about the center of a coordinate system defined by a well collimated beam of gamma radiation. A differential analyzer was set to accept only the photopeak of the

gamma ray involved. The measurement was repeated for gamma ray energies of .065 Mev, .129 Mev, .511 Mev, and 1.33 Mev with and without lateral lead shielding on the crystal. The integrands of α_0, α_2, and α_4 were plotted versus r and integrated by means of a compensating polar planimeter. Plots of α_2 and α_4 versus gamma ray energy for unshielded detectors are shown in Figures 14 and 15.

The effect of lateral shielding was not found to be significant except at low energies (< 100 Kev) where x-rays from the shielding material can enter the crystal. It should be noted, however, that the shielding can make an important contribution to the correction at higher energies if the differential analyzer is allowed to accept gamma rays which are compton-scattered from the shield.

The results of the present method for a gamma energy of .511 Mev were compared to results obtained by the annihilation correlation method of Church and Kraushaar.[49] The normalized attenuation coefficients, $(b_{\ell 0}/b_{00})^2$, for both methods are shown in Table III.

An examination of the results makes it clear that the method is valid for axial extensions of up to 1 to 2 cm (depending on the energy) for the source-to-detector distances studied. This is sufficient for most applications.

TABLE III

THE NORMALIZED ATTENUATION COEFFICIENTS, $(b_{20}/b_{00})^2$ AND $(b_{40}/b_{00})^2$ FOR A GAMMA RAY ENERGY OF .511 MEV AND r_0 = 9.90 CM

	$(b_{20}/b_{00})^2$	$(b_{40}/b_{00})^2$
Present Method	.931 ± .006	.787 ± .016
Method of Church and Kraushaar	.930 ± .006	.782 ± .015

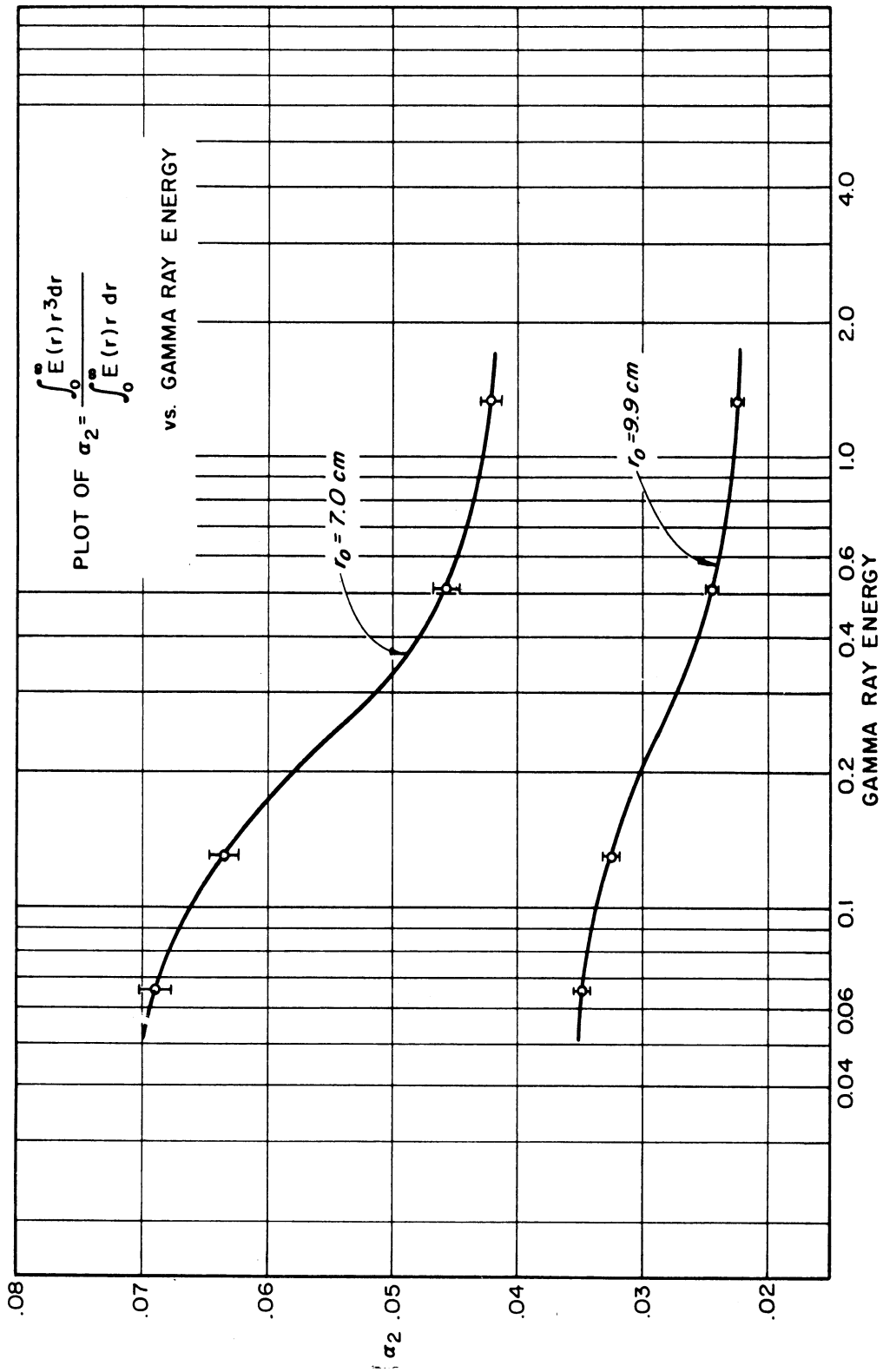

Fig. 14 Plot of α_2 vs. Gamma Ray Energy for r_o = 7.00 cm and r_o = 9.90 cm. The error limits represent our best estimate of the uncertainty in these measurements due to both random and systematic sources of error.

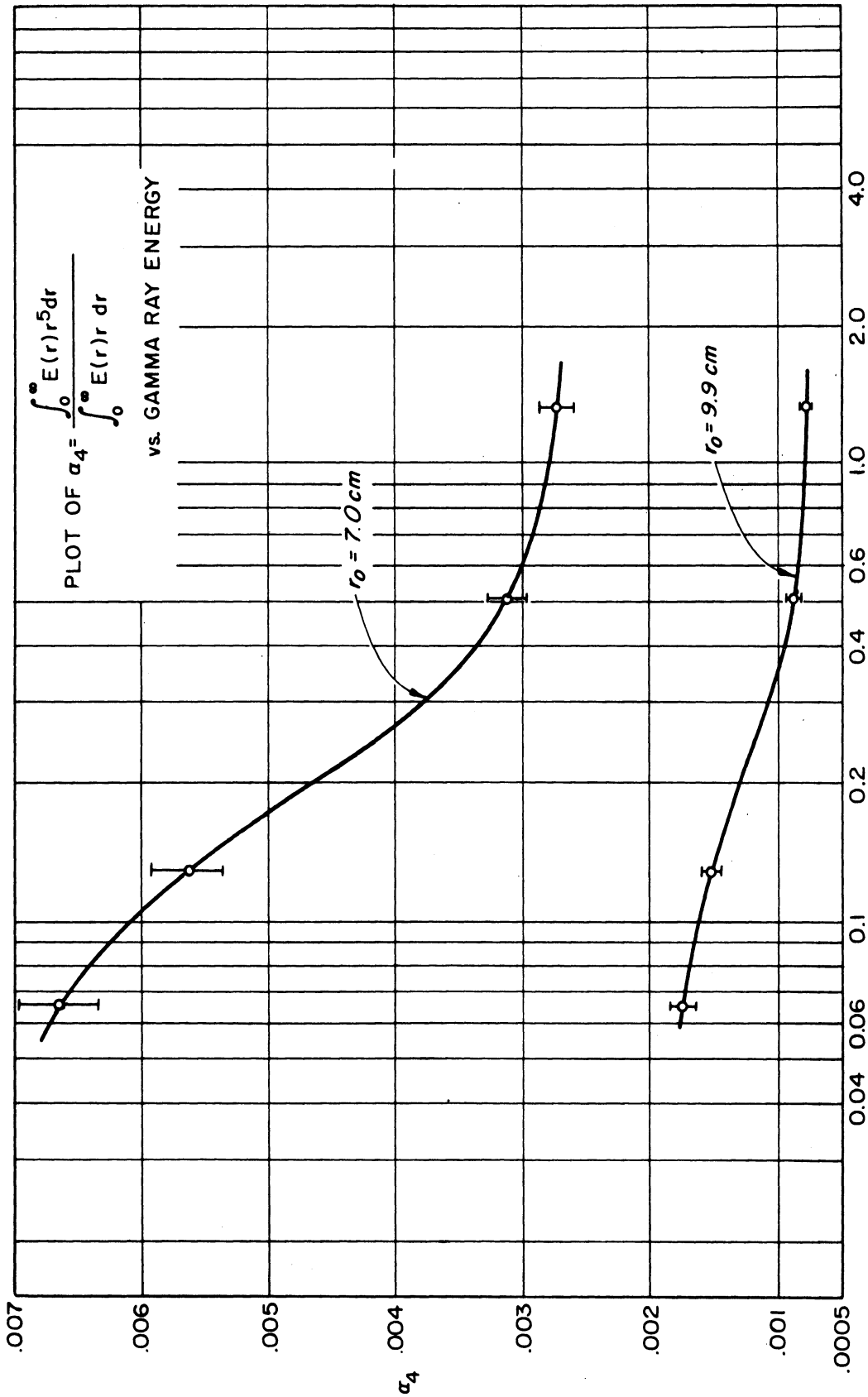

Fig. 15 Plot of α_4 vs. Gamma Ray Energy for r_o = 7.00 cm and r_o = 9.90 cm.

CHAPTER IV

EXCITED STATES OF EVEN-EVEN NUCLEI

Introduction

Recent studies of the level structure of even-even nuclei with a non-spherical equilibrium shape have given support to the existence of rotational and collective vibrational states as predicted by the unified model.[52,53] Two types of excitation have been postulated. The first involves collective motion in which the internal structure of the nucleus is preserved. The second mode is associated with the excitation of individual particles or with collective excitation of a group of nucleons. This latter type corresponds to vibrations about the equilibrium shape.

The theory of the rotational structure found in non-spherical nuclei has been well developed for axially-symmetric nuclei.[52-58] The motion is characterized by the quantum numbers, J, K, and M, representing the total angular momentum, its projection on the nuclear symmetry axis and its projection on the space-fixed axis, respectively. For the ground state of even-even nuclei, J = 0 +, K = 0 and the symmetrization of the wave function limits the rotational band to J = 0, 2, 4, 6, ..., all with even parity. For even-even nuclei, the energies of the rotational band are given by

$$E_{ROT} = \frac{\hbar^2}{2\tau} J(J+1) \qquad (1)$$

where τ, the moment of inertia, depends on the deformation and increases with the number of nucleons outside of closed shells. This model has

been successful in accounting for many features of the spectra of nuclei in the range of $A \sim 24$, $152 \leq A \leq 185$, and $A \geq 225$. The model has also been successful in predicting gamma and beta transition probabilities between rotational levels.[58,59] With decreasing deformation and increasing rotational frequency, the intrinsic nuclear structure is excited by the rotational motion and a strict adherance to the rotational spectrum is not to be expected. Slight changes occur in the positions of the energy levels and the selection rules governing transition probabilities become weakened.

Although the lowest collective excitations correspond to rotations with preservation of shape, nuclei may also exhibit collective excitations corresponding to vibrations about the equilibrium shape.[59] In axially symmetric nuclei the symmetry of the vibrations may be characterized according to their multipole order, λ, and ν, the component of the vibrational angular momentum along the symmetry axis. The excitation quanta, commonly called phonons, have total angular momentum λ, and parity $(-1)^{\lambda}$.

The quadrupole vibrations ($\lambda=2$) of the nucleus about a spheroidal equilibrium shape separate into two modes corresponding to $\nu=0$ (β-vibrations) and $\nu=2$ (γ-vibrations). Superimposed upon each vibrational state one expects to find a rotational band. The rotational band associated with the lowest mode of β-vibration ($n_\beta=1$, $n_\gamma=0$) has the same form as the ground state band, i.e., $K=0$, $J=0, 2, 4, \ldots$. The lowest γ-vibration band has the form $K=2$, $J=2, 3, \ldots$. Since the ellipsoidal shape is invariant under reflection through the origin, and the intrinsic structure in even-even nuclei has even parity, all quadrupole

vibrational levels have even parity. There are many cases of nuclear levels which can be ascribed to γ-vibrations. In the absence of a quantitative theory of γ-vibrations, this assignment is usually based on the spin values of these levels and on the enhancement of E2 transition probabilities (which confirms the collective nature of the excitation).

The lowest odd-parity modes (λ=3) may be characterized as octupole vibrations. Low-lying odd-parity states of this type have been observed in a number of even-even nuclei.[60] For K=0 or 1, these levels may have spins of 1, 3, 5, ... For K=2, spins of 2, 3, ... may be expected.[59]

As has been pointed out above, the unified model has been successful in predicting decay characteristics in the rotational regions. For intermediate region nuclei, i.e., nuclei outside the rotational regions and non-magic, systematic properties have likewise been observed. These nuclei generally have fewer nucleous outside of closed shells than rotational region nuclei. Goldhaber and Weneser[61] have proposed a spherical equilibrium model which assumes that the systematic excited levels are vibrational in character and arise from coupling of the spherical core to the outer nucleons. Ordinarily the first and second excited states of these nuclei have spin and parity of 2+. As the coupling increases, the excitation energy of the first excited state decreases and the ratio E_2/E_1 rises from an initial value of 2 to values greater than 2.2. The second excited state is a 3-fold multiplet with spins of 0, 2, 4; the third a 5-fold multiplet with spins of 0, 2, 3, 4, and 6. The E2 transition probability from the second 2+ state to the

first 2+ state is much larger than the single particle estimate. The crossover transition, i.e., from the second excited state to the ground state, is forbidden and can occur only as a failure of the oscillator approximation. Wilets and Jeans[62] have considered the case of anharmonic oscillations. They assume that the nucleus has a finite equilibrium deformation but is shape unstable. The energy associated with any ellipsoidal deformation depends only on the change in area of the nuclear surface to which it gives rise. The increase in surface area is related to a parameter β, while the shape is described by a parameter γ. They find a low-lying level structure similar to that proposed by Goldhaber and Weneser. In addition, the degenerate (0+, 2+, 4+) second excited state is now split with the 0+ level lying above the other two levels. Qualitative arguments by Marty[63], who assumed that the nucleus was a non-degenerate ellipsoid, have led to similar conclusions.

Recently, Davydov and Filippov have investigated the level structure of nuclei which do not possess axial symmetry.[64,65] They have regarded the nucleus as an asymmetric top and have investigated the rotational energy levels under the assumption that the internal state of the nucleus does not change during rotation. They have shown that the violation of axial symmetry only slightly affects the rotational spectrum of the axial nucleus. New levels with spins of 2, 3, 4, ..., appear which lie very high and are not excited if the deviation from axial symmetry is small. As the deviations from axial symmetry are increased these levels become much lower. Thus the ratio of the energy, E_{22}, of the second excited state with spin 2, to E_{21}, the energy of the first excited spin 2 state, varies from infinity to two. Davydov and

Filippov have calculated the positions of the low-lying states with spins of 2, 3, 4, 5, and 6 as a function of the deviation of the nucleus from axial symmetry. They also have calculated the electromagnetic transition probabilities between some of these states. A few of their results and experimental evidence supporting their conclusions will be presented in the following section.

Rotational State of Non-Axial Nuclei

Before discussing the specific case of non-axial nuclei, it is well to define some of the parameters which are necessary in order to gain some insight into the unified model. The following arguments are due to Bohr.[53]

Assume that the surface of the nucleus, $R(\theta,\phi)$, can be expanded as follows:

$$R(\theta,\phi) = R_o[1 + \sum_{\ell,m} a_{\ell,m} Y_{\ell,m}(\theta,\phi)] \qquad (2)$$

where R_o is the spherical nuclear radius. The function $Y_{\ell,m}(\theta,\phi)$ is the normalized spherical harmonic of order ℓ,m. If the deformation is small, the potential energy takes the form

$$V = 1/2 \sum_{\ell,m} C_\ell |a_{\ell,m}|^2 \qquad (3)$$

while the kinetic energy is given by

$$T = 1/2 \sum_{\ell,m} B_\ell |\dot{a}_{\ell,m}|^2 \qquad (4)$$

The quantities B_ℓ and C_ℓ depend on more detailed assumptions regarding the properties of nuclear matter. For the most part, it is only necessary to consider deformations of order 2(i.e. ℓ=2) which represent an

ellipsoid oriented in space. Instead of characterizing this deformation by the five coordinates a_{2m}, it may be described by three angular coordinates specifying the orientation of the ellipsoid and two internal parameters. The internal parameters are β, the deformation parameter, and γ, the shape parameter which are related by:

$$a_0 = \beta \cos \gamma,\ a_1 = a_{-1} = 0,\ a_2 = a_{-2} = (\beta/\sqrt{2}) \sin \gamma \qquad (5)$$

These are illustrated in Figure 16. The nuclear deformation is characterized by the point A in the two-dimensional polar diagram. The radius vector equals the deformation parameter β, and the polar angle is given by the shape parameter, γ. If A falls on the ξ-, η-, or ζ- axis, the nucleus possesses rotational symmetry with respect to its x'-, y'-, or z'- axis, respectively. (x', y', z' are the principal axes of the ellipsoid.) Hence the coordinate γ describes the deviation from rotational symmetry. For $\gamma = 0 + p\,\pi/3$, where p is an integer, two axes of the ellipsoid are equal. In these coordinates the potential energy becomes

$$V = 1/2\ C\ \beta^2 \qquad (6)$$

and it is customary to break the kinetic energy into the sum of a vibrational part and a rotational part:(53)

$$T_{vib} = -\frac{\hbar^2}{2B} \left\{ \frac{1}{\beta^4} \frac{\partial}{\partial \beta} \beta^4 \frac{\partial}{\partial \beta} + \frac{1}{\beta^2} \frac{1}{\sin 3\gamma} \frac{\partial}{\partial \gamma} \sin 3\gamma \frac{\partial}{\partial \gamma} \right\} \qquad (7)$$

$$T_{rot} = \sum_{\lambda=1}^{3} \frac{\hbar^2}{8B\beta^2} \frac{J_\lambda^2}{\sin^2 (\gamma - \frac{2\pi}{3} \lambda)} \qquad (8)$$

where the J_λ are the operators of the projections of the nuclear angular momenta on the axes of body-fixed system. Davydov and Filippov(64) have

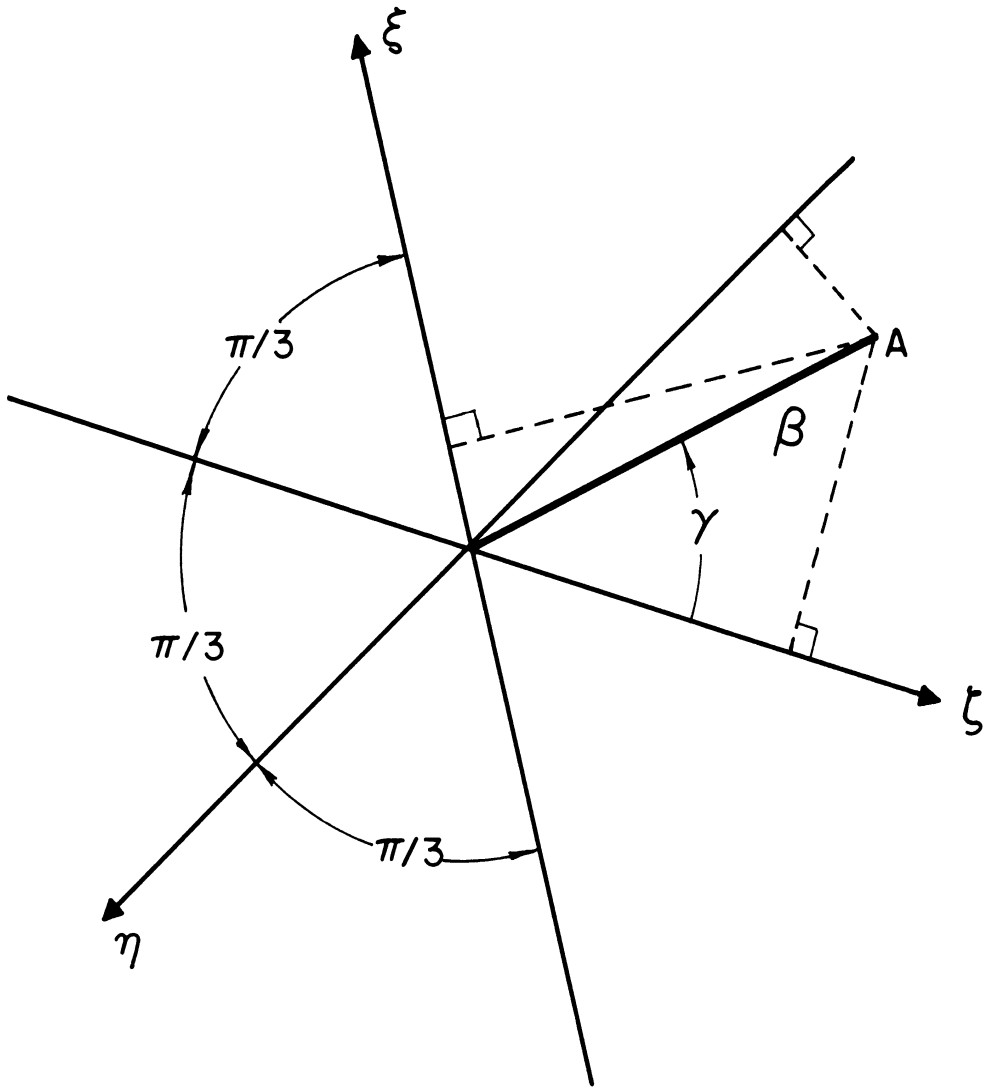

Figure 16. Internal Parameters of the Deformed Nucleus.

studied the rotational levels of the nucleus represented as an asymmetric top with rotational energy given by Equation (6). Each value of the total angular momentum of the asymmetric top corresponds to 2J+1 different energy levels. Since no symmetry axis exists, K is no longer a good quantum number. The asymmetric top has been treated quantum mechanically[66] and Davydov and Filippov have applied these results to the nuclear case. In virtue of the symmetry conditions imposed on the wave functions in even-even nuclei[53] only certain of the 2J+1 levels can occur. Thus rotational states of the required symmetry will not occur for J=1. Two such states will occur for J=2, one for J=3, three for J=4, etc. The relative energies of the low-lying rotational levels are shown in Figure 17 as a function of γ, the shape parameter. For γ=0, the energy spectrum is identical to that of an axially-symmetric nucleus. The energy levels are the same for γ_1 and $\pi/3 - \gamma_1$. Therefore the values of all quantities will be presented only in the interval between 0 and $\pi/6$ ($\gamma = 0°$ to $30°$). For a fixed value of β, violation of axial symmetry leads to a small increase in the energy of the levels of the axial nucleus. In addition violation of axial symmetry leads to the appearance of some new energy levels as shown in Figure 17. Note especially the second excited state with spin 2, the energy of which varies from infinity to twice the energy of the first spin 2 state. By using the dependence of this energy ratio, E_{22}/E_{21}, on γ, it is possible to estimate γ from the experimental ratio. The theory also predicts that the lowest spin 3 state will have an energy, E_3, which is given by

$$E_3 = E_{21} + E_{22} \qquad (9)$$

and which always lies above the lowest spin 4 state.

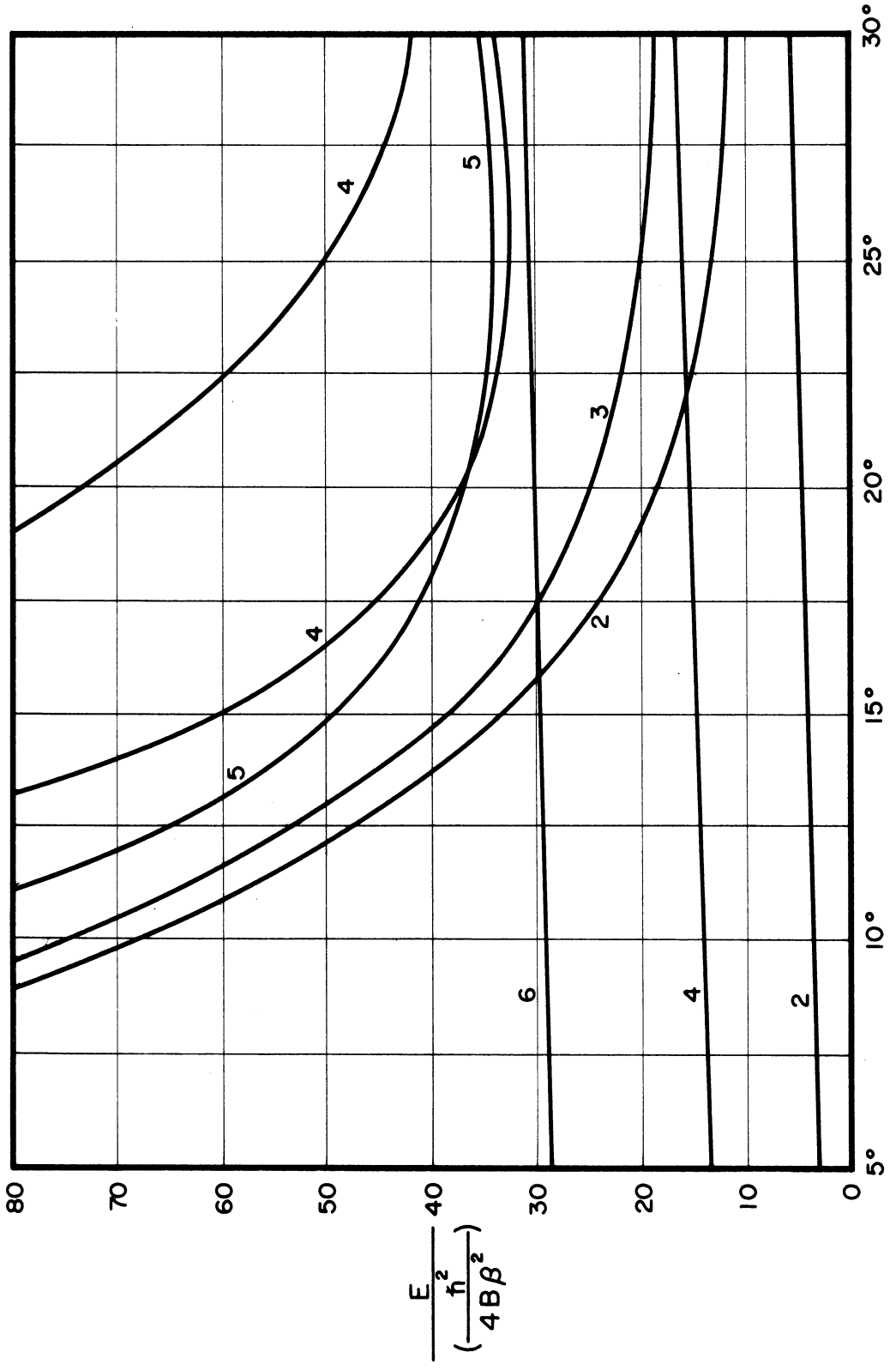

Figure 17. Rotational States of the Non-Axial Nucleus.

As was pointed out above, the first two levels with spin 2 observed in many intermediate region nuclei have been attributed in most cases to one-phonon and two-phonon vibrations of the nuclear surface. If this is indeed the case, the crossover, $22 \rightarrow 0$ (second spin 2 state to ground state), occurs only as a violation of the oscillator approximation. Moreover, M1 radiation is forbidden in the $22 \rightarrow 21$ transition. If these states are now to be interpreted as rotational, it is crucial to examine the electromagnetic transition probabilities between the rotational levels and to compare these predictions with experimental evidence. Davydov and Filippov have computed the E2 and M1 transition probabilities between the low-lying states. Their results are summarized in Table IV for electric quadrupole transitions. $b(E2; 22 \rightarrow 21)/b(E2; 22 \rightarrow 0)$ denotes the ratio of the reduced electric quadrupole transition probabilities for the cascade to the crossover in the 2 - 2 - 0 sequence. Note that the theoretical ratio varies from 1.43 for axial nuclei to ∞ for nuclei in which the deviation from axial symmetry is maximum.

Table V is a comparison of experimental evidence to the theoretical predictions for fourteen even-even nuclei. In each case the shape parameter, γ, has been determined from the ratio, E_{22}/E_{21}. Note that the first seven nuclei listed are from the intermediate regions while the last seven fall in the rotational regions. It is clear that the observed position of the lowest spin 3 level and the variation in the ratio of reduced cascade to crossover transition probability agree with the predicted values in both the intermediate regions and in the rotational regions.

TABLE IV

TRANSITION PROBABILITIES BETWEEN LOW-LYING ROTATIONAL LEVELS OF THE NON-AXIAL NUCLEUS

γ	$\frac{E_{22}}{E_{21}}$	$\frac{b(E2;\ 22 \rightarrow 21)}{b(E2;\ 22 \rightarrow 0)}$	$\frac{b(E2;\ 3 \rightarrow 21)}{b(E2;\ 3 \rightarrow 22)}$
0	∞	1.43	0
5	64.2	1.49	
10	15.9	1.70	.0075
15	6.85	2.70	.056
20	3.73	5.35	.072
22.5	2.93	9.01	
24	2.59	15.1	
25	2.41	20.6	.044
26	2.26	31.2	
28	2.07	126	
29	2.01	363	.039
30	2.00	∞	0

There are only two cases in which good experimental data exists to test the ratio of the reduced E2 transition probabilities between the spin 3 state and the two spin 2 states. The experimental ratio $b(E2: 3 \rightarrow 21)/b(E2: 3 \rightarrow 22)$ is equal to 0.016 in Kr^{82} and to 0.012 in Pt^{192}.(77,68) In each case the ratio E_{22}/E_{21} is slightly less than two, indicating $\gamma \sim 30°$. The theoretical ratio $b(E2: 3 \rightarrow 21)/b(E2: 3 \rightarrow 22)$

TABLE V

COMPARISON OF EXPERIMENTAL DATA TO THE THEORETICAL PREDICTIONS FOR NON-AXIAL NUCLEI

Nucleus	$\frac{E_{22}}{E_{21}}$	γ	Experimental Energies (Mev)		$\frac{b(E2;\ 22 \rightarrow 21)}{b(E2;\ 22 \rightarrow 0)}$		Reference
			$E_{21} + E_{22}$	E_3	Theor.	Exp.	
Pt^{196}	1.97	30	1.040	-	∞	> 2500	67
Ge^{72}	1.75	30	2.30	-	∞	358	Chap. VI
Pt^{192}	1.94	30	.929	.921	∞	172	68
Xe^{128}	2.0	30	1.445	-	∞	197	69
Te^{122}	2.25	26.5	1.76	1.76	66	78.2	70
Hg^{198}	2.66	23.2	1.50	-	13	25	71
Os^{188}	4.10	18.9	.788	(.785)	4.3	3.2	72
W^{186}	8.08	13.9	1.00	1.00	2.0	-	73
Gd^{154}	8.12	13.8	1.133	1.140	1.9	1.9	74
Sm^{152}	8.9	13.5	1.206	1.226	1.9	1.7	78
Dy^{160}	11.0	12.2	1.051	1.047	1.9	2.2	Chap. V
W^{182}	12.0	11.6	1.322	1.331	1.6	1.6	75
Pu^{238}	23.4	8.1	1.074	1.076	1.2	1.4	76
Pu^{240}	23.7	8.0	1.063	1.060	1.2	-	73

varies from .036 to 0 between $\gamma=29°$ and $\gamma=30°$ in agreement with the observed values.

The calculations of Davydov and Filippov have also lead to a prediction of the E2 and M1 mixture in the 22 $\rightarrow$ 21 transition. The ratio of E2 intensity to M1 intensity, δ^2, is given by

$$\delta^2 = 2/3\ Z^2\ A^{4/3}\ (E_{22} - E_{21})^2 \times 10^{-4} \qquad (10)$$

where the energy is in Mev. Note that δ^2 is independent of the shape parameter, but it must be borne in mind that this equation is only to be applied to deformed nuclei. The theoretical line and data from eight measured mixing ratios are shown in Figure 18. All of the mixtures shown are based on directional correlation measurements in 2 - 2 - 0 cascades. It is extremely difficult to obtain a precise value for δ^2 in most cases and the graph shows only that the experimental data do not disagree with the proposed model.

It is well to remember that the calculations of Davydov and Filippov were based on the assumption that the internal state of the nucleus does not change during rotation. This is an approximation, especially for the intermediate region nuclei where the lowest rotational levels have an energy comparable to internal excitation levels. This "strong coupling" or "adiabatic" approximation is probably not well satisfied for the first three nuclei listed in Table V or for some of the higher excited states of the other nuclei listed.

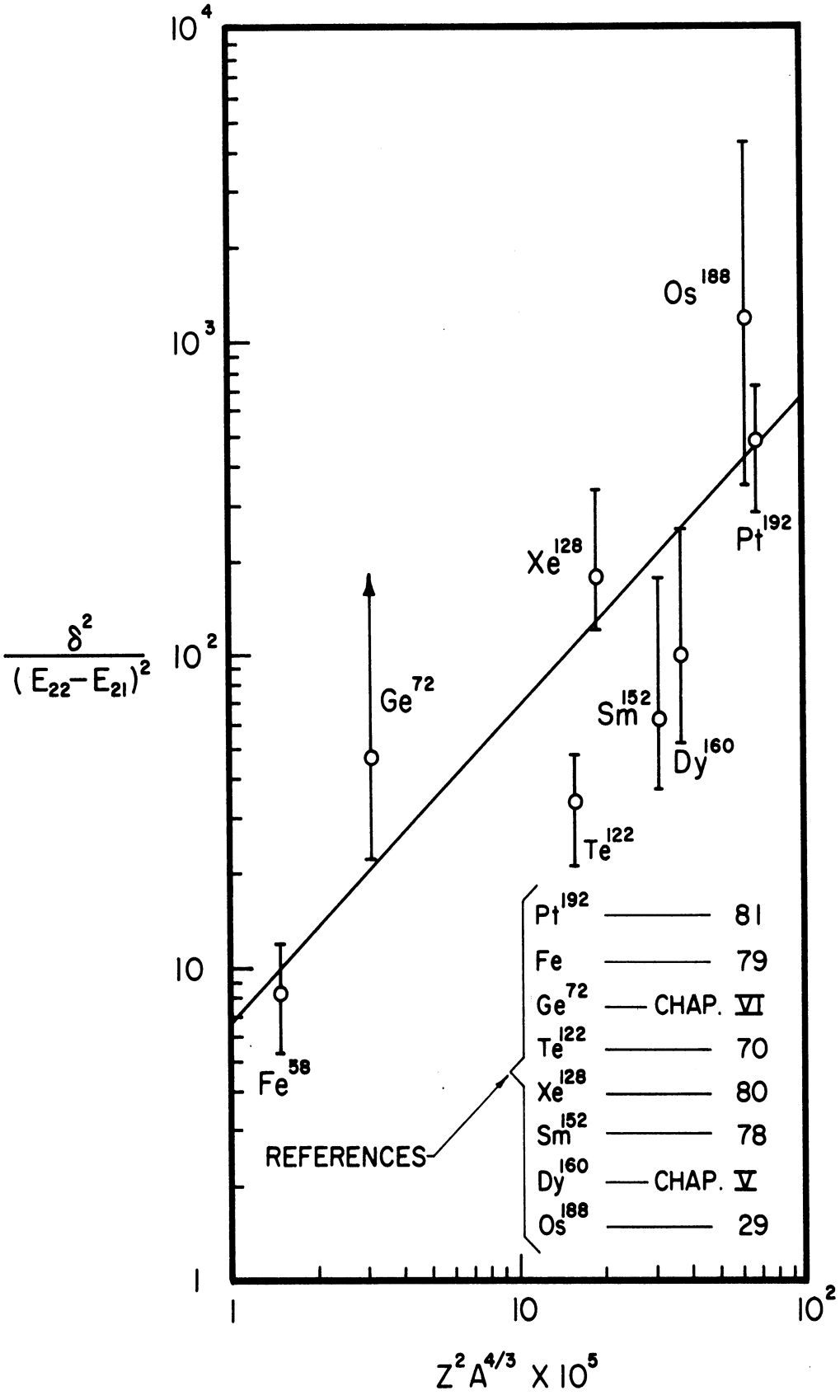

Figure 18. Mixing Ratio for 22 → 21 Transition in Some Deformed Nuclei.

CHAPTER V

DIRECTIONAL CORRELATION OF GAMMA RAYS IN Dy^{160}

Introduction

The level structure of Dy^{160} following beta decay of the 72 day Tb^{160} has been the subject of several investigations.[82-92] The more recent of these studies have been in agreement on many features of the level structure in Dy^{160}. Before the present investigation was undertaken, conflicts still existed in regard to the relative intensities and multipolarities of several gamma transitions. The directional correlation of the 1.076 Mev - .196 Mev cascade reported by Ofer[83] was considerably different from that observed by Nathan.[82] In addition, Ofer found it necessary to postulate an attenuation[83,92] in interpreting three of his directional correlation measurements (those involving the .087 Mev level). Under the circumstances an attenuation is difficult to understand and further study of this aspect was thought to be of value. Thus the present coincidence and directional correlation measurements were undertaken in the hope of resolving some of the incompatible aspects of previous research on this decay.

Dy^{160} is situated in a region of strongly deformed nuclei and exhibits a characteristic ground state band with spins of 0+, 2+, and 4+. The higher excited states of Dy^{160} have been interpreted as quadrupole and octupole vibrational levels.[82] It would now seem possible to reinterpret two of these higher levels as rotational based on the asymmetric top model discussed in Chapter IV. Hence an accurate knowledge of relative intensities and multipole mixtures is important in order to compare the predictions of these two interpretations of the unified model.

High purity Tb_2O_3 powder was irradiated for 24 hour periods in the University of Michigan Ford Nuclear Reactor. The activated powder was then dissolved in HCl and the solution was diluted. No impurity activities were found to be present in the source material.

Results and Interpretation

Coincidence Measurements

The gamma-ray spectrum of Tb^{160} is shown in Figure 19. In order to determine the position of the various gamma rays in the decay scheme, measurements were made of the gamma rays coincident with the following energy regions:

$$0.080 \text{ Mev} \leq E \leq 0.100 \text{ Mev}, \quad 0.160 \text{ Mev} \leq E \leq 0.240 \text{ Mev},$$

$$0.250 \text{ Mev} \leq E \leq 0.350 \text{ Mev}, \text{ and } 0.830 \text{ Mev} \leq E \leq 1.00 \text{ Mev}.$$

The qualitative results are summarized in Table VI.

A knowledge of the relative intensities of the 0.877, 0.960 and 0.964 Mev lines is necessary in order to interpret the angular correlation data. Hence a careful measurement was made by means of the 0.298 Mev coincidence spectrum. After correction for detector efficiency and the slight overlap of the lines, the intensity ratio 0.877: 0.964: 0.960 was found to be $1 : 0.73 \pm 0.06 : 0.29 \pm 0.06$. This ratio was confirmed by measurements in the 0.087 Mev coincidence spectrum although the presence of interfering cascades prevented reliable quantitative results. The present results are in good agreement with the ratio $1 : 0.68 \pm 0.10 : 0.35 \pm 0.10$ found by Nathan. A ratio of $1 : 0.90 \pm 0.18 : 0.05 \pm 0.01$ has been quoted by Ofer.

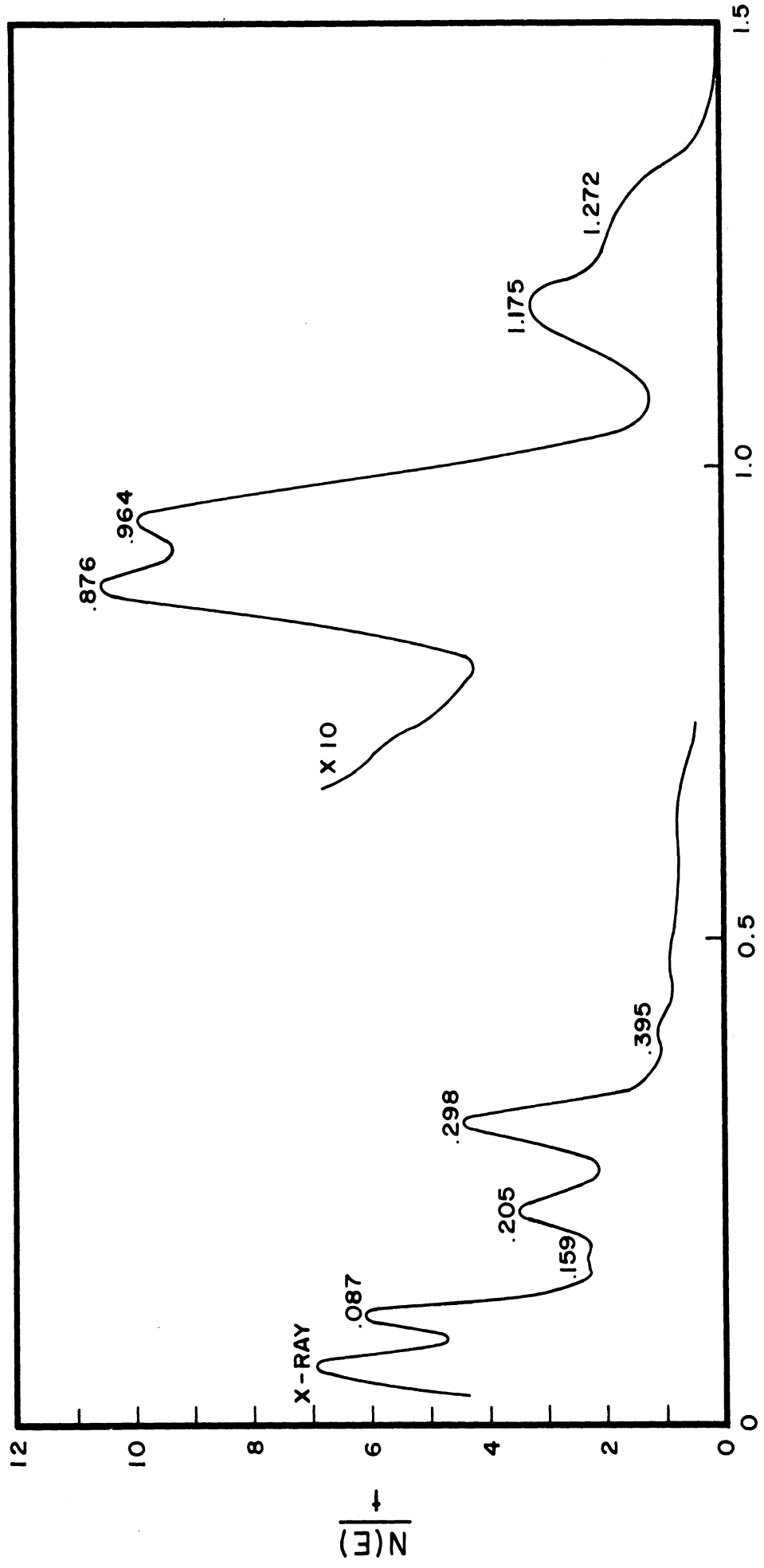

Figure 19. Gamma Ray Spectrum of Tb^{160}.

TABLE VI

GAMMA-GAMMA COINCIDENCE MEASUREMENTS IN Dy^{160}

Energy Region (Mev)	Transitions Selected (Mev)	Coincident Transitions (Mev)	Remarks
$0.080 \leq E \leq 0.100$	0.087	0.196 + 0.215, 0.298, 0.877, 0.960, 1.175, 1.272	The photopeak at 0.960 Mev was found to be about 1/3 as strong as the 0.876 Mev photopeak after subtraction of intefering cascades.
$0.160 \leq E \leq 0.240$	0.196, 0.215	0.087, 0.196 + 0.215, 0.298, 0.681, 0.764	The 0.681 Mev transition was found to be about 1/2 as strong as the 0.764 Mev transition. No gamma ray was found at 1.047 Mev thus ruling out the presence of a strong ground state transition from the 1.047 Mev level.
$0.250 \leq E \leq 0.350$	0.298	0.087, 0.196, 0.877, 0.964	The 0.964 Mev transition was found to be about 2/3 as strong as the 0.877 Mev transition.
$0.830 \leq E \leq 1.00$	0.877, 0.960, 0.964	0.087, 0.159, 0.215, 0.298	

The decay scheme shown in Figure 20 is due to Nathan.[82] The relative intensities of some transitions have been modified to agree with the present measurements. An additional level at 1.200 Mev and several weak transitions have been added to the scheme on the basis of internal conversion measurements by Grigor'ev et al.[88]

Table VII shows the principal results of the internal conversion measurements as measured by Grigor'ev et al.[88] The theoretical values listed are taken from the tables of Sliv.[28]

TABLE VII

INTERNAL CONVERSION MEASUREMENTS IN Dy^{160}

E_γ (Mev)	α_K(exp) (x 10^3)	Theoretical α_K			
		E1	E2	M1	M2
.087	1300	380	1600	3100	29000
.215	43	34	130	240	1100
.298	14	15	49	98	390
.876	2.9	1.4	3.4	6.2	16
.960	2.5	1.1	2.8	5.0	12
.964	2.5	1.1	2.8	5.0	12
1.172	.64	.81	1.9	3.1	7.5
1.200	.87	.79	1.8	3.0	7.2
1.272	.54	.69	1.6	2.6	6.2

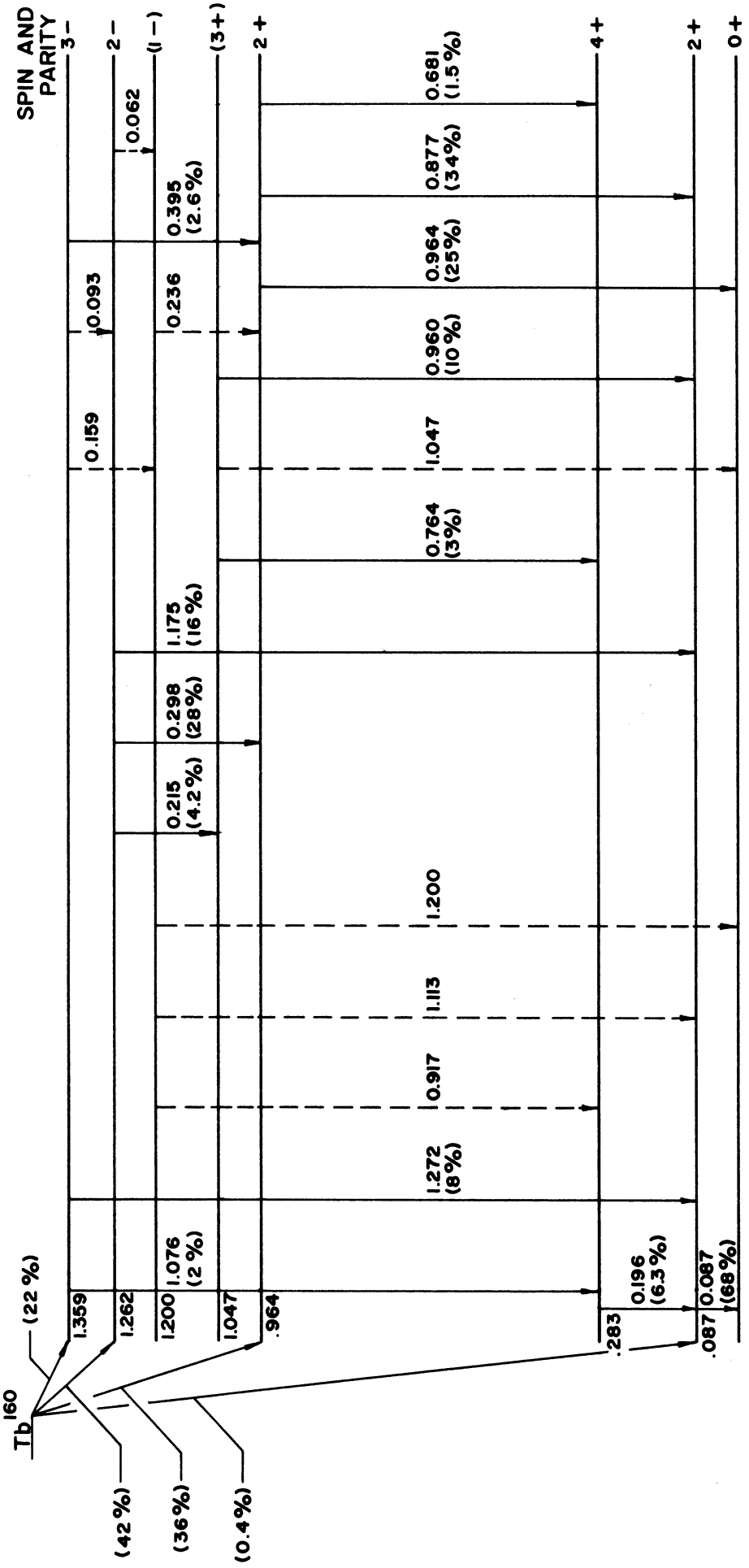

Figure 20. Decay Scheme of Tb^{160}. The beta decay data and gamma ray energies (in Mev) are according to Nathan. The relative intensities are due to Nathan except where directly measured in the present research.

0.298 Mev - 0.877 Mev and 0.298 Mev - 0.964 Mev Directional Correlations

Although the 0.877 Mev photopeak and the 0.960 Mev and 0.964 Mev combined photopeak were easily resolved by the scintillation counters, there remains a small overlap of these lines which must be considered in analyzing the angular correlation data. Two angular correlation measurements were made. In each measurement one of the differential analyzers was set to accept the upper half of the photopeak of the 0.298 Mev gamma ray. In one case the second differential analyzer was set to accept a narrow range of pulses in the upper half of the 0.964 Mev photopeak. In the other measurement, the second differential analyzer selected a narrow range of energies centered on the 0.877 Mev photopeak.

Using the measured relative intensities (without the detector efficiency correction), the 0.877 Mev and 0.964 Mev photopeaks were constructed from known shapes of single gamma rays in this energy region. The integrated contribution of both gamma rays to each correlation function was then determined. The two correlation functions were combined with special attention to the errors in the relative intensities, channel settings, and the correlation functions themselves. In this manner the 0.298 Mev - 0.964 Mev angular correlation yielded expansion coefficients $A_2 = + 0.259 \pm 0.042$ and $A_4 = - 0.031 \pm 0.030$. Figure 21 shows the experimental points and least squares curve before correction along with the correlation curve after correction (dotted curve). The corrected coefficients are in good agreement with the theoretical coefficients for a pure 2(D)2(Q)0 cascade, i.e., $A_2 = + 0.250$, $A_4 = 0$. If the cascade is of the form 2(D,Q)2(Q)0, the limits of error will allow a maximum of 0.5% quadrupole content in the 0.298 Mev transition. This assignment is

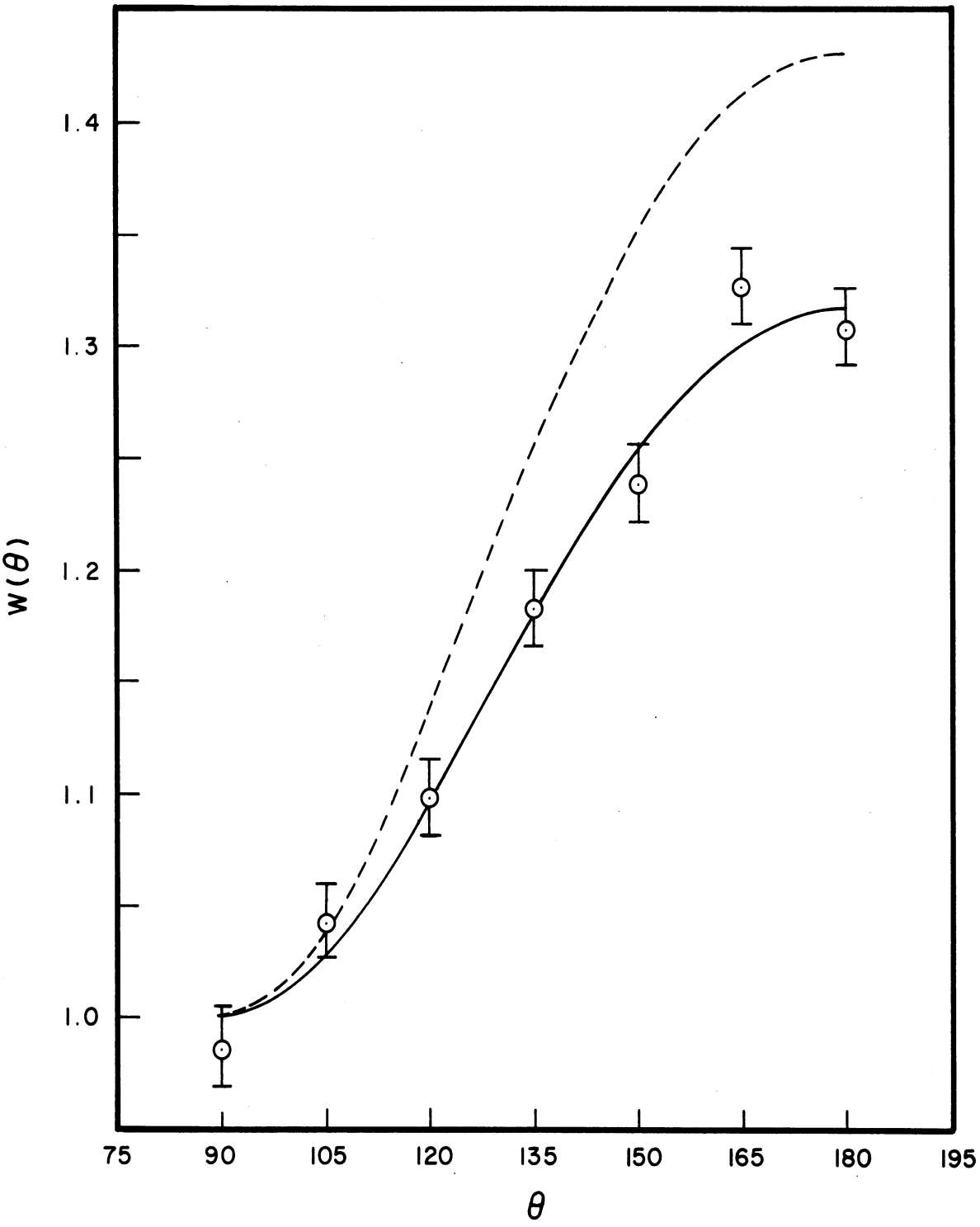

Fig. 21 Correlation Function for the 0.298 Mev - 0.964 Mev Cascade.

supported by the measured K-conversion coefficients[82,88] which indicate an E1 multipolarity for the 0.298 Mev gamma ray and E2 for the 0.964 Mev transition. It seems safe to assign a spin and parity of 2+ to the 0.964 Mev level on the basis of the conversion data. The expansion coefficients for this sequence are also consistent with a 3(D,Q)2(Q)0 cascade with a quadrupole content Q_1 for the first transition of $0.21 \leq Q_1 \leq 0.65$. An M2 content of this magnitude is inconsistent with experience and with the measured K-conversion coefficients. Thus a spin assignment of 3 must be ruled out for the 1.262 Mev level.

In the manner described above the corrected expansion coefficients for the 0.298 Mev - 0.877 Mev sequence were found to be $A_2 = -0.126 \pm 0.026$ and $A_4 = +0.015 \pm 0.020$. The first excited state (at 0.087 Mev) can almost certainly be characterized as 2+. If the 0.298 Mev transition is assumed to be pure dipole, the data are then consistent with a 2(D)2(D,Q)2 sequence with $0.95 \leq Q_2 \leq 0.99$ or $0.25 \leq Q_2 \leq 0.35$. The latter possibility can be ruled out by the angular correlation data from the 0.877 Mev - 0.087 Mev cascade which is given below. The possibility of a small M2 admixture in the 0.298 Mev transition cannot be ruled out. The graphical analysis of the data for a doubly mixed cascade is shown in Figure 22 in which the range of E1 + M2 mixture for the 0.298 Mev transition is assumed from the results of the 0.298 Mev - 0.964 Mev correlation. Again in accord with the results of the 0.877 Mev - 0.087 Mev angular correlation, the data still require a quadrupole content of $0.925 \leq Q_2 \leq 0.995$ for the 0.877 Mev transition.

In summary, it has been shown that the 0.298 Mev gamma ray proceeds from a 2- level at 1.262 Mev to a 2+ level at 0.964 Mev by radiation which is predominantly electric dipole ($\leq 0.5\%$ M2). The

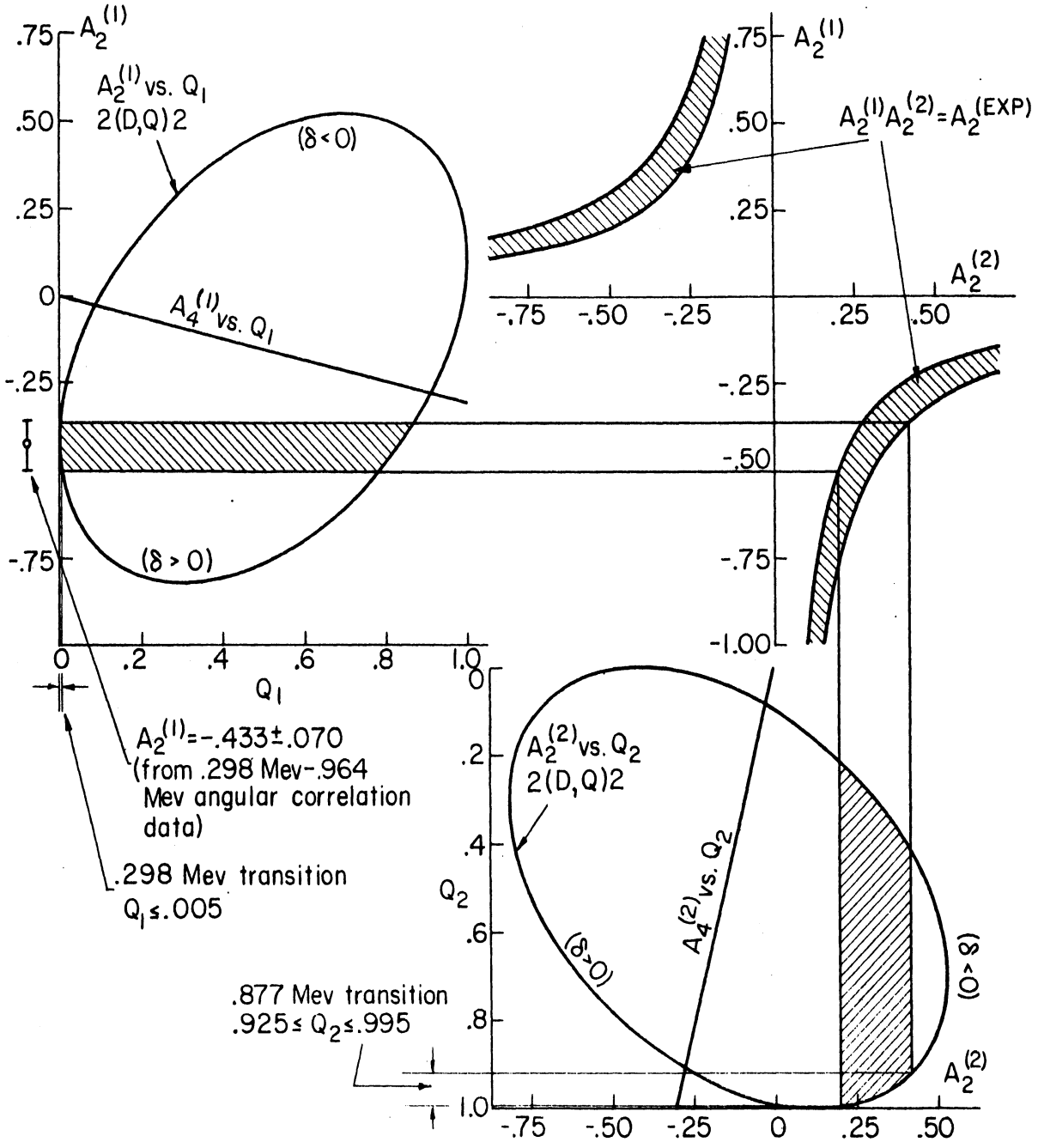

Figure 22. Analysis of the 0.298 Mev - 0.877 Mev Directional Correlation in Terms of a 2(D,Q)2(D,Q)2 Sequence.

0.964 Mev level decays by pure E2 radiation to the 0+ ground state and by 96 + 3.5% E2 and 4 $\mp$ 3.5% M1 radiation (0.877 Mev gamma ray) to the 2+ first excited state at 0.087 Mev.

0.877 Mev - 0.087 Mev Directional Correlations

The 0.877 Mev gamma ray is a transition from the 2+ level at 0.964 Mev to the first excited state (spin and parity of 2+) at 0.087 Mev. Angular correlation measurements on this cascade can provide information on the multipolarity of the 0.877 Mev transition, assuming that the 0.087 Mev transition is pure E2. An accurate measurement is not possible, however, due to the presence of the Compton distributions of interfering cascades. The chief contributions to this background, i.e., the 1.272 Mev - 0.087 Mev, 1.175 Mev - 0.087 Mev, 0.960 Mev - 0.087 Mev, and 0.298 Mev - 0.877 Mev cascades, comprise nearly 50% of the real coincidences measured by accepting a small portion of the 0.087 Mev and 0.877 Mev photopeaks in alternate differential analyzers. However, the range of multipolarities possible for the 0.877 Mev gamma ray is already known from the 0.298 Mev - 0.877 Mev angular correlation measurement. Thus, despite the large errors introduced by the interference subtraction, the 0.877 Mev - 0.087 Mev data can be used to distinguish between the two allowable ranges. After correction for the interference, the expansion coefficients were found to be $A_2 = -0.10 \pm 0.08$ and $A_4 = +0.27 \pm 0.09$. Within the rather large experimental errors, these coefficients require an E2 content of $Q \geq .975$ in the 0.877 Mev gamma ray.

The angular correlation of this cascade was also measured by Ofer.[83] In that measurement the experimental data were corrected for interference from the 1.272 Mev - 0.087 Mev and 1.175 Mev - 0.087 Mev

cascades and the resultant coefficients were considerably smaller than would be expected for the large quadrupole admixture present in the 0.877 Mev transition. The present measurements indicate that it is not necessary to postulate an attenuation if all interference is considered. However, the presence of some attenuation cannot be ruled out. Ofer and Cohen[92] were unable to achieve a completely satisfactory explanation for the large attenuation proposed. It will be seen below that the results of the 1.272 Mev - 0.087 Mev and 1.175 Mev - 0.087 Mev angular correlations can be more readily understood if no attenuation is present.

1.272 Mev - .087 Mev and 1.175 Mev - .087 Mev Directional Correlations

The 1.175 Mev and 1.272 Mev photopeaks are barely resolved in the scintillation spectrum, and an analysis similar to that employed for the 0.298 Mev - 0.877 Mev and 0.298 Mev - 0.964 Mev correlations must be applied in order to obtain the corrected angular correlation functions. The errors involved are large due to a poor knowledge of the relative intensities and are reflected in the increased error limits of the expansion coefficients. The corrected expansion coefficients for the 1.175 Mev - 0.087 Mev angular correlation were found to be $A_2 = + 0.133 \pm 0.041$ and $A_4 = + 0.008 \pm 0.083$. Similarly the 1.272 Mev - 0.087 Mev cascade yielded $A_2 = + 0.148 \pm 0.065$ and $A_4 = - 0.09 \pm 0.14$.

The 1.175 Mev gamma ray proceeds from the 2- level at 1.262 Mev to the first excited state. The cascade is certainly of the form 2(D,Q)2(Q)0. The expansion coefficients are then consistent with an E1 + M2 mixture for the 1.175 Mev gamma ray with $97.5 \pm 1.5\%$ E1 and $2.5 \mp 1.5\%$ M2. This is in agreement with the K-conversion coefficient

measurements of Nathan and of Grigor'ev et al. If a perturbation were present, a larger M2 content could not be ruled out. Assuming an attenuation, Ofer's data[83] would require an M2 content of about 65%. This would contradict the conversion measurements and also constitute a much larger M2 admixture than is normally encountered. Hence the results tend to favor the present interpretation.

The 1.272 Mev gamma ray is a transition from a level at 1.359 Mev to the first excited state. Of the spin assignments logically available for the 1.359 Mev level, the angular correlation data is consistent only with 2 or 3. As will be shown below, the 1.076 Mev - 0.196 Mev angular correlation rules out a spin assignment of 2 for the 1.359 Mev level. For a 3(D,Q)2(Q)0 sequence the data require $0.04 \leq Q_1 \leq 0.18$ or $0.66 \leq Q_1 \leq 0.86$. The K-conversion coefficient measured by Nathan favors an E1 multipolarity for the 1.272 Mev transition. Hence the 1.359 Mev level is most naturally characterized as 3 - and the 1.272 Mev gamma ray is an E1 + E2 mixture with $89 \pm 7\%$ E1 and $11 \mp 7\%$ M2. Ofer, assuming a perturbation, found a quadrupole content of between 27% and 50% for the 1.272 Mev transition.

1.076 Mev - 0.196 Mev Directional Correlation

The 1.076 Mev gamma ray is a transition from the 1.359 Mev level to the second excited state at 0.283 Mev. The 0.196 Mev gamma ray is a transition between the second and first excited states. Both gamma rays involved are very weak. The window of one differential analyzer was set to accept the 0.205 Mev photopeak and the other was set with a narrow window in the region where the 1.076 Mev gamma ray should occur. After

correction for finite resolution the expansion coefficients were found to be $A_2 = + 0.273 \pm 0.020$ and $A_4 = -0.092 \pm .032$. It was found that interference was present due to the high energy tails of the 0.960 Mev and 0.964 Mev gamma rays as the 0.215 Mev - 0.960 Mev and the 0.298 Mev - 0.964 Mev cascades. No adequate method could be found for subtracting out this interference.

It seems highly probable that the second excited state can be characterized as 4+. Of the possible sequences 4(D,Q)4(Q)2, 2(Q)4(Q)2, and 3(D,Q)4(Q)2, the first two require a positive A_4 coefficient. The present data, even with the large interference, require an A_4 which is negative. Thus a spin of 3 must be assigned to the 1.359 Mev level. If the form of the interference correlations is taken into consideration, the expansion coefficients limit the quadrupole content of the 1.076 Mev gamma ray to $Q \leq .20$.

Summary and Discussion

Gamma rays in Dy^{160} following beta decay of the 72-day Tb^{160} have been studied using coincidence and directional correlation methods. A consistent decay scheme has been proposed, in agreement with the principal features of the scheme proposed by Nathan.[82] Directional correlation measurements have been made on the 0.298 Mev - 0.964 Mev, 0.298 Mev - 0.877 Mev, 0.877 Mev - 0.087 Mev, 1.272 Mev - 0.087 Mev, 1.175 Mev - 0.087 Mev, and 1.076 Mev - 0.196 Mev cascades. The spin and parity of the 0.087 Mev, 0.964 Mev, and 1.262 Mev levels were found to be 2+, 2+, and 2- respectively. The measurements favor spins of 4 for the 0.283 Mev level and 3 for the 1.359 Mev level. The 0.298 Mev gamma ray was found

to be pure dipole radiation ($Q \leq .005$). The 0.876 Mev gamma ray was shown to be largely E2 with a small M1 admixture. The 1.175 Mev, 1.272 Mev, and 1.076 Mev gamma rays were found to be mostly dipole (probably E1) with a small quadrupole admixture. The data are consistent with an E2 character for the 0.964 Mev, 0.087 Mev and 0.196 Mev gamma transitions.

Dy^{160} is situated in a region of strongly deformed nuclei and the ground state, 0.087 Mev, and 0.283 Mev levels form the expected ground state rotational band with spins of 0+, 2+, and 4+, respectively. If the rotating nucleus is assumed to be axially symmetric, the higher excited levels at 0.964 Mev, 1.047 Mev, 1.200 Mev, 1.262 Mev, and 1.359 Mev are most easily interpreted as electric quadrupole and octupole vibrational states. Associated with these states one expects to find a rotational sequence of states in which the separation between the first and second member is of the same order of magnitude as in the ground state band.[59] Each rotational band is characterized by the quantum number K (projection of the total angular momentum on the nuclear symmetry axis). If one considers the energies, spins, and parities of the higher excited states, it is possible to interpret all of the higher excited states as vibrational in character. The two even parity states at 0.964 Mev and 1.047 Mev may be interpreted as the first two members of a gamma vibrational band with K=2. The weakly fed level at 1.200 Mev probably has a spin and parity of 1- and may be interpreted as the first member of a K=0 octupole vibrational band. The 2- and 3- levels at 1.262 Mev and 1.359 Mev appear to be the first two members of a K=2 octupole vibrational band. The K values assigned have been discussed by Nathan.[82] The relative intensities predicted by the unified model agree fairly well with the experimental observations.

If the rotating nucleus is considered as a non-axial ellipsoid, it is possible to interpret the 2+ and 3+ levels at 0.964 Mev and 1.047 Mev as belonging to the ground state rotational band. It is interesting to compare these two interpretations of the unified model with the experimental evidence. Both versions of the model agree on the positions of these two levels. The ratio E_{22}/E_{21} corresponds to a shape parameter of $\gamma=12.2°$. The ratio of the reduced transition probabilities for transitions from the 2+ levels are compared in Table VIII.

TABLE VIII

COMPARISON OF TRANSITION PROBABILITIES FROM THE 0.964 MEV LEVEL IN Dy^{160}

	Symmetric Nucleus	Asymmetric Nucleus	Exp.
$\frac{b(E2;\ 22 \rightarrow 21)}{b(E2;\ 22 - 0)}$	1.4	1.9	$2.2 \pm .2$

The results of the 0.298 Mev - 0.877 Mev and 0.877 Mev - 0.087 Mev directional correlations indicate that the 0.877 Mev transition is mostly E2 with a small (.5% - 7.5%) M1 admixture. If a symmetric top were a good description of the nucleus, and if the 0.964 Mev level were indeed characterized by K=2, the M1 transition would be highly forbidden. A small M1 content is usually observed in transitions of this type in the rotational nuclei and is an indication that K is not a good quantum number. The asymmetric top model predicts an M1 content of 0.5% in this transition. Hence there would seem to be some evidence that Dy^{160} can be adequately described as a non-axial nucleus.

CHAPTER VI

DIRECTIONAL CORRELATION OF GAMMA RAYS IN Ge^{72}

Introduction

The levels in Ge^{72} following beta decay of the 14.2 hour Ga^{72} have been studied by a number of investigators.[93-103] The beta- and gamma-ray spectra were investigated in detail by Kraushaar et al.[101] and independently by Johns et al.[100] Important features of the level structure were confirmed by studies of the decay of As^{72}.[104]

The first excited state of Ge^{72} has spin zero and even parity.[95-97] This represents a departure from the usual 2+ first excited state found in even-even nuclei. The only other known exceptions (O^{16}, Ca^{40}, Zr^{90}, and Pb^{208}) apparently result when both neutrons and protons form closed shells. This anomolous state has an energy of 0.69 Mev above the ground state.[101] It decays to the ground state by internal conversion with a lifetime of 0.3 microseconds. It was felt that direct measurement of the spins of some of the higher levels might be of value in establishing the relation of this unusual state to the level structure of Ge^{72}. Moreover, these measurements can be useful in comparing the structure of Ge^{72} to the systematics of other nuclei in this region.

The main features of the decay are shown in Figure 23. Many weak gamma rays and transitions involving the 0+ first excited state have been omitted for the sake of clarity. The complete level structure (including transitions fed from Ga^{72} and As^{72}) is shown in Figure 24.[105] The numbers in parentheses under the gamma energies in Figure 24 are the branching percentages from the level. Figure 25 shows the gamma ray spectrum.

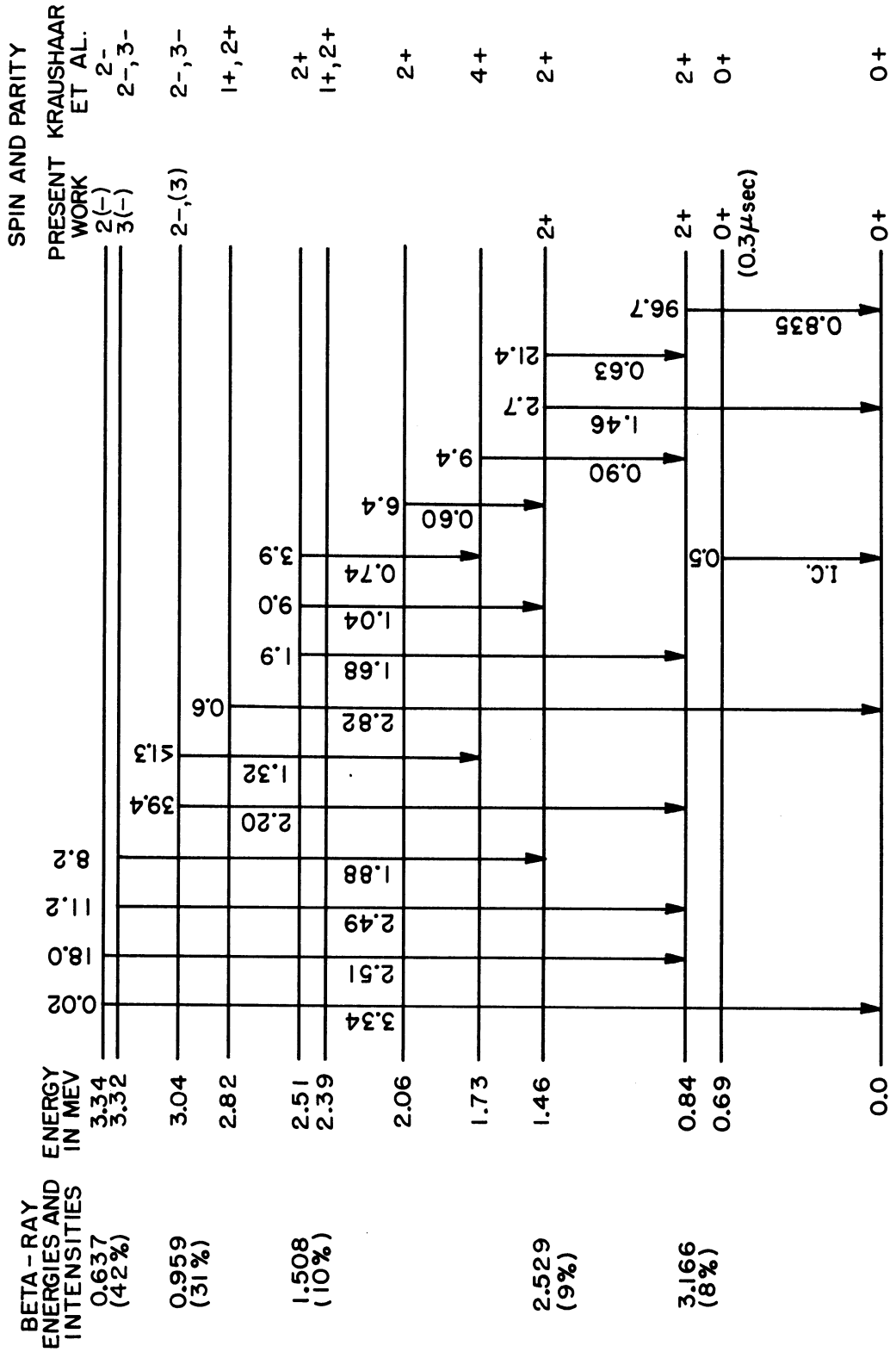

Fig. 23 Simplified Decay Scheme of Ga^{72}.

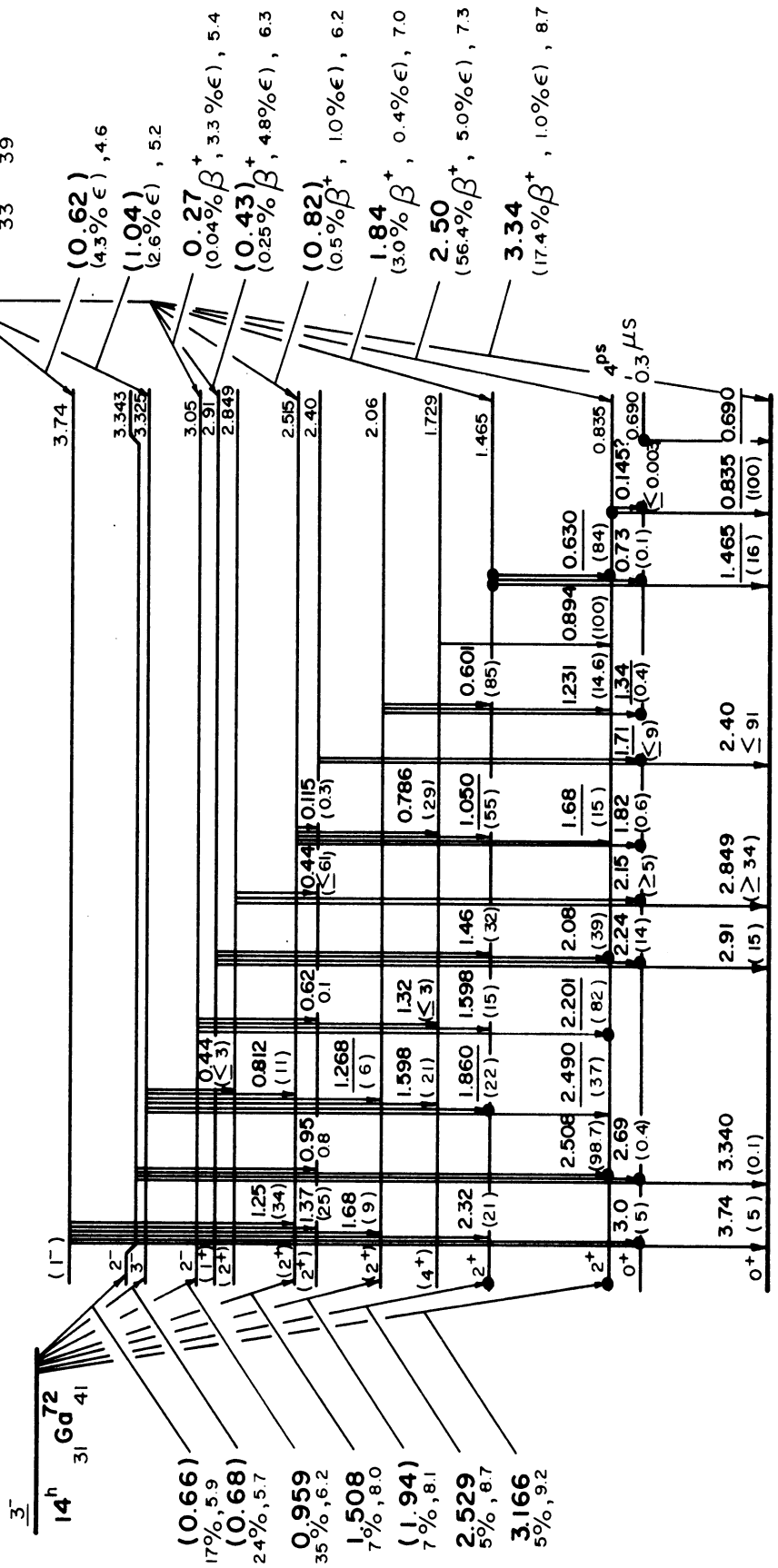

Figure 24. Level Structure of Ge^{72}.

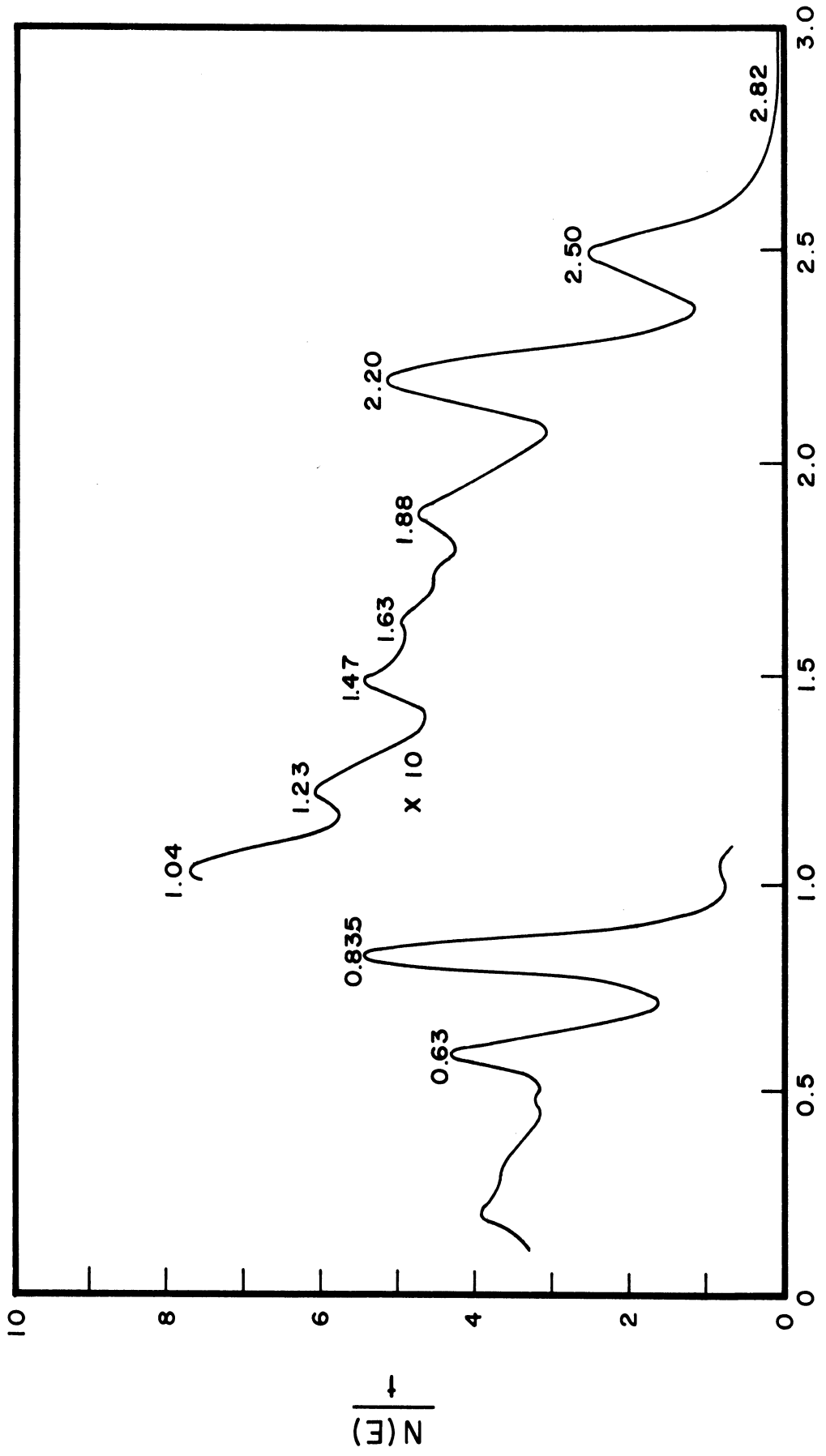

Figure 25. Gamma-Ray Spectrum of Ga^{72}.

In the present investigation, directional correlation measurements were made on the 0.63 Mev - 0.835 Mev, 2.49 and 2.51 Mev - 0.835 Mev, 2.20 Mev - 0.835 Mev, and 1.88 Mev - 1.46 Mev gamma ray cascades. The Ga^{72} source material was obtained from Oak Ridge National Laboratory as gallium chloride in a dilute HCl solution. Sources were prepared by diluting this material and sealing the solution in lucite source holders. The decay of the gamma spectrum was followed for several half-lives. No interfering activities were found.

The half-life of the 0.835 Mev level has been measured to be $(3.2 \pm 0.8) \times 10^{-12}$ seconds by Metzger(106) using resonant scattering techniques. From energy considerations, the half-life of the 1.46 Mev level is expected to be at least as short. These lifetimes, together with the fact that the source was in dilute solution, eliminates the possibility of attenuation of the correlation due to extranuclear fields.

Results and Interpretation

0.63 Mev - 0.835 Mev Directional Correlation

The directional correlation of this cascade was measured by accepting all coincidences in a narrow portion of the scintillation photopeak for each of the gamma rays. However, owing to the complexity of the decay scheme, a fair percentage of these coincidences result from other interfering cascades. It was found that coincidences between the 0.835 Mev gamma ray and the Compton distribution of higher energy gamma rays resulted in $20.5 \pm 2.1\%$ of the total real coincidences. Similarly coincidences between the 0.63 Mev gamma ray and Compton distributions beneath it with the Compton distribution of higher energy gamma rays were found to comprise $23.4 \pm 2.5\%$ of the total coincidences. The interfering

correlations were measured and subtracted from the main correlation function. Initially 3000 real coincidences were collected at seven angles in each quadrant for the basic correlation. The experiment was repeated at four angles in each quadrant and 7000 real coincidences were collected at each angle. The two measurements agreed within experimental error. The resulting expansion coefficients, after correction for the interfering cascades, were found to be $A_2 = - 0.145 \pm 0.040$ and $A_4 = + 0.314 \pm 0.065$. The directional correlation of this cascade was also measured by Coleman.[103] After corrections similar to those described above, he found expansion coefficients of $A_2 = - 0.096 \pm 0.130$ and $A_4 = + 0.49 \pm 0.21$. The latter work agrees with the present investigation within the large error limits quoted by Coleman. It should be noted that the corrected expansion coefficients still contain contributions from coincidences between the 0.835 Mev gamma ray and the weak 0.60 Mev and 0.74 Mev gamma rays. No correction can be made for this interference.

Metzger has shown that the 0.835 Mev level has a spin of 2 by studying the angular distribution of resonance radiation from this level.[106] It was found that the present experimental data could not be fit by sequences of the form 4(Q)2(Q)0, 3(D,Q)2(Q)0, or 1(D,Q)2(Q)0. The data are in agreement with a 2(D,Q)2(Q)0 sequence in which the 2(D,Q)2 transition (0.63 - Mev gamma ray) is mostly quadrupole with a small dipole admixture. The experimental coefficients for the first cascade are compared to the theoretical 2(D,Q)2 mixture curve in Figure 26. The 0.835 Mev transition has been assumed to be a pure 2(Q)0 transition and the experimental expansion coefficients have therefore been divided by the corresponding F-coefficients [$F_2(2,0,2,2) = - .5976$ and $F_4(2,0,2,2) = 1.069$]. It is seen that the experimental coefficients correspond to a

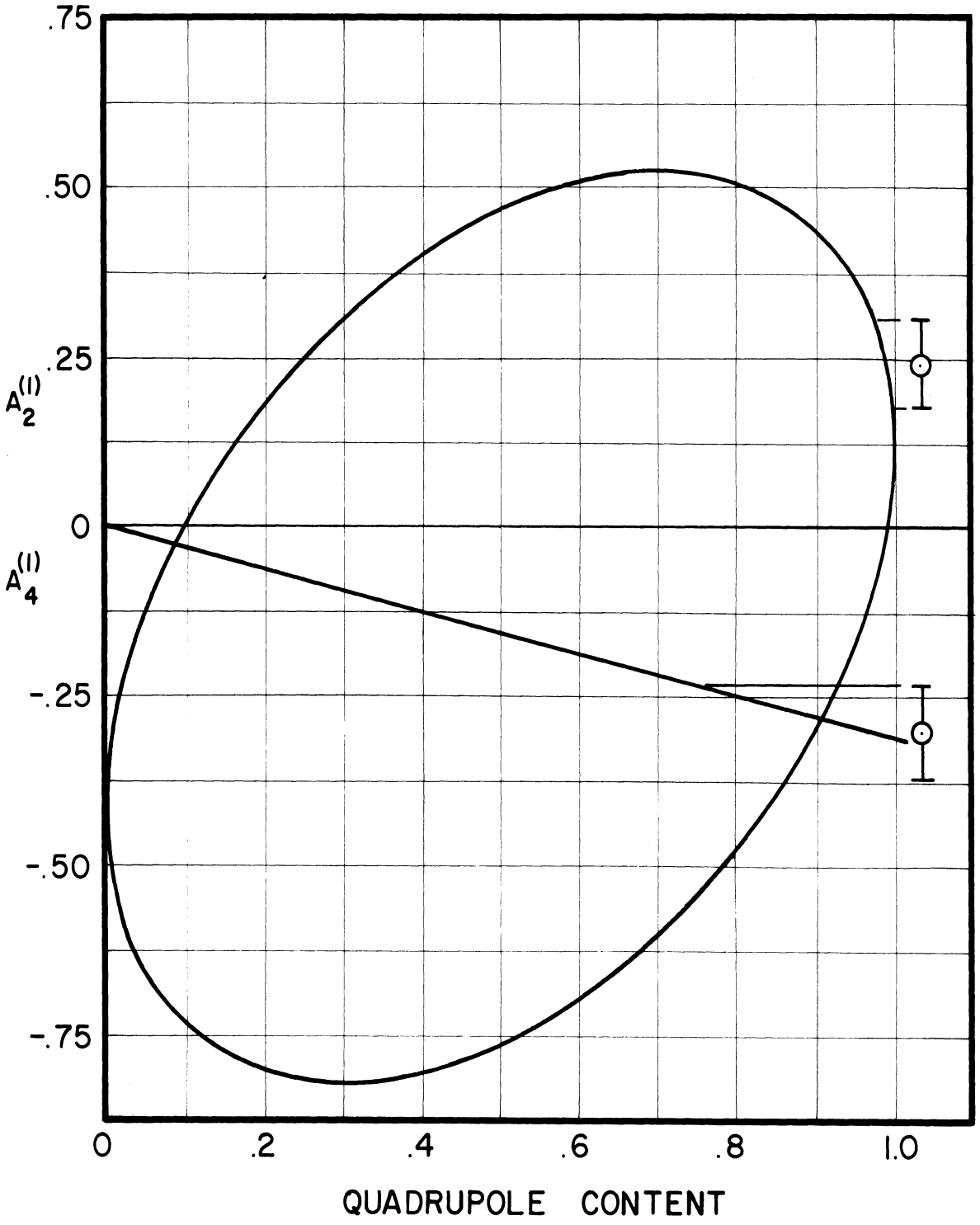

Figure 26. $A_2^{(1)}$ and $A_4^{(1)}$ vs. Q for a 2(D,Q)2 Sequence.

quadrupole intensity for the 0.63 Mev transition of $Q \geq 0.975$. If reasonable values are assumed for the maximum effect on the results due to our ignorance of the contribution from the interfering 0.60 Mev 0.835 Mev and 0.74 Mev - 0.535 Mev cascades, the amended coefficients still demand a quadrupole intensity of $Q \geq 0.90$.

2.49 and 2.51 Mev - 0.835 Mev
Directional Correlation

Although it is not possible to resolve the 2.49 Mev and 2.51 Mev gamma rays by means of a scintillation detector, these transitions have been separated by photoelectric conversion. In this manner Hedgran and Lind found a intensity ratio of 2.51 Mev: 2.49 Mev:: 8:5.[107] The directional correlation of both gamma rays with the 0.835 Mev transition was measured by accepting the full-energy peak of the combined 2.49 Mev and 2.51 Mev gamma rays in one differential analyzer and the 0.835 Mev gamma ray in the other. The experimental expansion coefficients for this directional correlation were found to be $A_2 = + 0.163 \pm 0.031$ and $A_4 = - 0.133 \pm 0.046$. There were no interfering cascades. A weak cross-over transition has been observed and has been assigned to the 3.34 Mev level although it may originate from the other or both levels. However, it is very weak ($\sim$.001) compared to the cascade intensity and this would rule out a spin 1 assignment for the levels at 3.32 Mev and 3.34 Mev. Assuming reasonable errors for the relative intensities of these cascades, all possible combinations of spins 2, 3, or 4 were considered as assignments for the 3.32 Mev and 3.34 Mev levels. The experimental data were found to be consistent only with spin 2 for one level and spin 3 for the other (in either order), with spin 3 for both levels, or with

spin 3 for one level and spin 4 for the other. Relative intensity considerations favor quadrupole radiation for the ground-state transition (i.e., the 3.34 Mev gamma ray). If this is indeed the case, it must originate from a spin 2 level and the directional correlation data then require a spin of 3 for other level.

2.20 Mev - 0.835 Mev Directional Correlation

This directional correlation was measured by accepting the photopeaks of the 2.20 Mev and 0.835 Mev gamma rays in separate energy channels. A portion of the real coincidences accepted in higher energy channel were due to the Compton and escape peaks of the 2.49 Mev and 2.51 Mev gamma rays. A fair estimate of the contribution (23.7 $\pm$ 2.4%) was obtained by moving the window of the differential analyzer from the 2.20 Mev photopeak to the valley between it and the 2.50 Mev photopeak and comparing coincidence rates. This percentage was then used directly in subtracting the interfering correlation from the observed correlation for the present cascade. Although the assumptions involved are crude, the observed correlations are very similar and as a result the corrected coefficients are not very sensitive to the actual contribution.

After correction for the interfering cascades, the experimental coefficients were found to be $A_2 = + 0.250 \pm 0.024$ and $A_4 = - 0.008 \pm 0.032$. These are in excellent agreement with the theoretical coefficients for a pure 2(D)2(Q)0 sequence. The error limits on the expansion coefficients in this case will allow no more than 0.1% quadrupole admixture. The experimental coefficients will also fit a 3(D,Q)2(Q)0 sequence with $0.23 \leq Q \leq 0.32$ for the mixed transition.

1.88 Mev - 1.46 Mev Directional Correlation

The directional-correlation of this very weak cascade was measured by accepting the full-energy peak of each gamma ray in separate differential analyzers. There were no interfering cascades. The resultant coefficients, $A_2 = + 0.010 \pm 0.051$ and $A_4 = - 0.055 \pm 0.074$ are consistent with sequences of the form 1(D,Q)2(Q)0, 2(D,Q)2(Q)0, or 3(D,Q)2(Q)0. (The spin of the 1.46 Mev level has been assumed to be 2 from the results of the 0.63 Mev - 0.835 Mev correlation.) The absence of a strong cross-over transition eliminates the first possibility.

Summary and Discussion

Directional correlation measurements have been made on the 0.63 - 0.835 Mev, 2.20 - 0.835 Mev, 2.49 and 2.51 - 0.835 Mev and 1.88 - 1.46 Mev gamma-gamma cascades in Ge^{72}. The level at 0.835 Mev has a spin and parity of 2+ and proceeds to the 0+ ground state by pure electric quadrupole radiation. The 0.63 Mev transition has been shown to proceed from a 2+ level at 1.46 Mev to the 0.835 Mev level by radiation which is largely electric quadrupole with a small magnetic dipole admixture. The correlation data favor a spin of 2 for the 3.04 Mev level, although a spin of 3 cannot be ruled out. The data are consistent with spin assignments of 2 or 3 for the levels at 3.32 Mev and 3.34 Mev.

The ground-state angular momentum of Ga^{72} has been shown to be 3.[108] The careful studies of the beta and gamma ray spectra of Ga^{72} and As^{72} have lead to the spins and parities shown in Figure 24.[101,104] These are in agreement with the present measurements for all levels studied

in the present work. Van Patter has summarized the systematics of even-even nuclei in this region.[109] The energy ratio of the second to the first excited state was shown to be less than 2 over the range $30 \leq N \leq 40$. If the 0+ first excited state of Ge^{72} is omitted, the energy ratio of the next two states ~ 1.75. Over the range $32 < N < 50$, the spin of the second excited state is 2+ in all known cases, omotting the low-lying 0+ states in Ge^{70} and Ge^{72}. The enhancement of the electric quadrupole transition probability in the 2 - 2 transition which was found in the present case is also characteristic of the 2 - 2 - 0 cascades in other nuclei in this region.

In terms of the asymmetric top model of Davydov and Filippov (Cf. Chapter IV), the fact that the energy ratios $E_{22}/E_{21} = 1.75$ would imply a large deviation from axial symmetry. Unfortunately, the assumption that the rotational level energy is small compared to the intrinsic excitation energy is not fulfilled in this case. This may explain the lowering of the second excited state in this region ($30 \leq N \leq 40$). The 0.835 Mev level has been reached by coulomb excitation.[110] The observed enhancement of the E2 transition probability to this state (F=18) would indicate that this level is a result of collective excitation. The large E2 content of the transition between the 1.46 Mev level and the 0.835 Mev level supports the conclusion that these states are of a collective nature. If a large shape parameter is assumed, say $\gamma \geq 28$, the other properties of the excited states can be compared on the basis of the unified model. Consider first the intensity of the crossover transition from the 1.46 Mev level to the ground state. The experimental relative intensities of the 0.63 Mev and 1.46 Mev gamma rays lead to a ratio of

the reduced E2 transition probabilities of $b(E2;\ 22 \rightarrow 21)/b(E2;\ 22 \rightarrow 0)$ of 358. From Table IV the theoretical ratio is greater than 126 for $\gamma \geq 28$. The theoretical considerations of Chapter IV would require a quadrupole content of $Q = .889$ for the 0.63 Mev gamma ray. The experimentally determined content has been shown to be $Q \geq .90$. The feeding of the level at 1.73 Mev has led to a spin and parity assignment of 4+ to this level. It is interesting to note that Figure 17 of Chapter IV predicts a 4+ level slightly above the second 2+ level for $\gamma \geq 22$. The level at 1.73 Mev may then be a 4+ rotational level.

The present work did not include any direct measurements involving the 0+ first excited state in Ge^{72}. However, it has been shown that various features of the Ge^{72} level structure are in good agreement with the systematics of even-even nuclei in this region if the 0+ state is ignored. This state does not appear to be connected with the low-lying collective states and hence is probably attributable to an intrinsic excitation. Ge^{72} has 32 protons and 40 neutrons. One may speculate that the $p_{1/2}$ neutron subshell and the $p_{3/2}$ proton subshell are filled in Ge^{72} and the excitation to the 0+ state may result from raising a proton pair or a neutron pair to a higher configuration. The near degeneracy of the $2p_{3/2}$ and $1f_{5/2}$ nucleon configurations may be associated with this anomolous state.

CHAPTER VII

FUTURE DEVELOPMENTS

In addition to the two nuclei reported in this dissertation, a number of other even-even nuclei are being investigated in this laboratory. The study of even-even nuclei has contributed significantly to our knowledge of the nucleus in general. However, much more information must be gathered before the systematics of this class of nuclei can be considered as well-established. At present there are a number of models which seek to explain the systematics of even-even nuclei. Before a decision can be made regarding the ability of any model to explain nuclear behavior, additional work by both theorists and experimentalists will be necessary. The theorists must predict more properties of the nuclear level structure on the basis of the model, and remove some of the restrictive assumptions which have hitherto limited the application of models. In this respect the work of Davydov and Filippov has merit in that it successfully predicts more properties of nuclear structure and is applicable to all deformed nuclei, rather than to a specific class of deformed nuclei. Its weakness is its failure to consider rotational - vibrational interaction and rotational - particle interaction. The experimentalist must provide a more complete picture of nuclear systematics in order to provide a means of testing the model. In this respect, a careful study of the positions, spins and parities of low-lying nuclear levels, together with the transition probabilities between these levels, would seem most important. A fruitful approach at present would seem to be careful measurements of the E2 content in 22 $\rightarrow$ 21 transitions, together

with more careful observations of the ratio of reduced transition probabilities, $b(E2; 22 \rightarrow 21)/b(E2; 22 \rightarrow 20)$. As more detailed predictions become available, other properties will require examination.

In odd-A nuclei, the doubly-mixed cascade is quite common and this, together with the variety of ground-state spins, has limited the application of directional correlation methods. However, many ground-state spins have now been measured. This, and the application of the method outlined in Chapter II, thus make it possible to obtain unique assignments from directional correlation experiments. A number of odd-A nuclei are now being studied with the hope of eventually establishing a systematic pattern for this class of nuclei.

In addition to the study of low-lying energy levels, it is important to see that higher excited states exhibit a systematic behavior which is consistent with the behavior at lower energies. To this end it may be possible to apply coincidence and angular correlation techniques to the prompt gamma rays which accompany thermal neutron capture.

In order to facilitate the study of low-lying nuclear levels, a number of improvements have been made in the coincidence and directional correlation apparatus. A 256-channel analyzer has been acquired which greatly facilitates the study of gamma ray singles and coincidence spectra. Several new circuits have been provided for the directional correlation apparatus in order to improve the stability and reliability of the apparatus. An automatic data recording system is now in use which allows data to be collected continuously.

It is felt that the continued application and extension of directional correlation techniques can do much to improve our knowledge

of nuclear energy levels. It is hoped that the representation of the nucleus by a consistent model, along with the discoveries of high-energy nuclear physics, will eventually provide the clues necessary to lead to a rigorous theory of the nucleus.

BIBLIOGRAPHY

1. Hamilton, D. R. Phys. Rev., 58, (1940), 122.

2. Brady, E. L. and Deutsch, M. Phys. Rev., 72, (1947), 870.

3. Brady, E. L. and Deutsch, M. Phys. Rev., 74, (1948), 1541

4. Goertzel, G. Phys. Rev., 70, (1946), 897

5. Falkoff, D. L. Doctoral Thesis, University of Michigan, 1948.

6. Falkoff, D. L. and Uhlenbeck, G. E. Phys. Rev., 79, (1950), 323.

7. Ling, D. S. and Falkoff, D. L. Phys. Rev., 76, (1949), 1639.

8. Racah, G. Phys. Rev., 84, (1951), 910.

9. Fano, U. Phys. Rev., 90, (1953), 577.

10. Lloyd, S. P. Phys. Rev., 85, (1952), 904.

11. Alder, K. Helv. Phys. Acta, 25, (1952), 235.

12. Coester, F. and Jauch, J. Helv. Phys. Acta, 26, (1953), 3.

13. Frauenfelder, H. in Beta and Gamma Ray Spectroscopy. North-Holland Publishing Co., 1955.

14. Wigner, E. P. Gruppentheorie. Braunschweig: F. Vieweg und Sohn, 1931.

15. Heitler, W. Quantum Theory of Radiation. New York: Oxford University Press, 1944.

16. Yang, C. N. Phys. Rev., 74, (1948), 764.

17. Biedenharn, L. C. and Rose, M. E. Revs. Mod. Phys., 25, (1953) 729.

18. Ferentz, M. and Rosenzwieg, N. ANL-5324, 1955.

19. Jastram, Wood, and Hurley. Bull. Am. Phys. Soc. Ser. II, 3, (1958), 65.

20. Coleman, C. F. Nuclear Phys., 5, (1958), 495.

21. Rose, M. E. Phys. Rev., 91, (1953), 610.

22. Arns, R. G. and Wiedenbeck, M. L. University of Michigan Research Institute, Technical Report 2375-3-T, January, 1958.

23. Klema, E. D. Phys. Rev., 109, (1958), 1652.

24. McGowan, Klema, and Bell. Phys. Rev., 85, (1952), 152.

25. Marmier, P. and Boehm, F. Phys. Rev., 97, (1955), 103.

26. Speck, D. R. and Jenkins, F. A. Phys. Rev., 101, (1956), 1831.

27. Heydenberg, N. P. and Temner, G. M. Phys. Rev., 100, (1955), 150.

28. Sliv, L. A. and Band, I. M. Leningrad Physico-Technical Report, (1956) translation. Report 57 ICC K1, issued by Physics Department, University of Illinois, Urbana, Illinois.

29. Wiedling, Tor. Directional Correlation Measurements and Some Other Related Investigations of Excited Nuclei. (Almquist and Wiksells Boktryckeri AB, Uppsala, 1956)

30. Schiff, L. I. Phys. Rev., 50, (1936), 88.

31. DeBenedetti, S. and Findley, R. W. in Handbuch der Physik. XLV, (Springer-Verlag, 1958), 236 ff.

32. Bell, R. E., Graham, R. L., and Petch, H. E., Canad. J. Phys., 30, (1952), 35.

33. Bernstein, W., Chase, R. L., and Schart, A. W. Rev. Sci. Instr., 24, (1953),437

34. Chase, R. L. BNL-263, 1953.

35. Pound, R. V. and Abragam, A. Phys. Rev., 90, (1953), 993.

36. Abragam, A. and Pound, R. V. Phys. Rev., 92, (1953), 943.

37. Frankel, S. Phys. Rev., 83, (1951), 673.

38. Frauenfelder, H. in Beta and Gamma Ray Spectroscopy. North-Holland Publishing Co., (1955), 599.

39. Scharenberg, R. P. Doctoral Thesis, University of Michigan, 1955.

40. Stewart, M. G. Doctoral Thesis, University of Michigan, 1955.

41. Garwin, R. L. Rev. Sci. Instr., 21, (1950), 569.

42. Garwin, R. L. Rev. Sci. Instr., 24, (1953), 618.

43. Johnstone, C. W. Nucleonics, 11, (1953), 36.

44. Lu, D. C. Doctoral Thesis, University of Michigan, 1954.

45. Klema, E. D. and McGowan, F. K. Phys. Rev., 92, (1953), 1469.

46. Walter, Huber, and Zunti. Helv. Phys. Acta, 23, (1950), 697.

47. West, H. I., Jr., UCRL-5451, 1958.

48. Lawson, J. S., Jr. and Frauenfelder, H. Phys. Rev., 91, (1953), 649.

49. Church, E. L. and Kraushaar, J. J. Phys. Rev., 88, (1952), 419.

50. Feingold, A. M. and Frankel, S. Phys. Rev., 97, (1955), 1025.

51. Schiff, L. I. Quantum Mechanics. New York: McGraw-Hill Book Co., 1955.

52. Bohr, A. and Mottelson, B. R. Mat. Fys. Medd. Dan. Vid. Selsk., 27, No. 16, 1953.

53. Bohr, A. Mat. Fys. Medd. Dan. Vid. Selsk., 26, No. 14, 1952.

54. Filippov, G. F. Dok. Akad. Nauk SSSR, 115, (1957) 696.

55. Davydov, A. S. and Chaban, A. A. JETP, 33, (1957), 547.

56. Davydov, A. S. and Filippov, G. P. JETP, 33, (1957), 723.

57. Davydov, A. S. and Murashkin, B. M. JETP, 34, (1958), 1619.

58. Alaga, Alder, Bohr, and Mottelson. Mat. Fys. Medd. Dan. Vid. Selsk., 29, No. 9, 1955.

59. Alder, Bohr, Huus, Mottelson, and Winther. Revs. Mod. Phys., 28, (1956), 432.

60. Sund, Arns, and Wiedenbeck. Bull. Am. Phys. Soc. Ser. II, 4, (1959), 292.

61. Scharff-Goldhaber, G. and Weneser, J. Phys. Rev., 98, (1955), 212.

62. Wilets, L. and Jeans, M. Phys. Rev., 102, (1956), 788.

63. Marty, C. Nuclear Phys., 3, (1952), 193.

64. Davydov, A. S. and Filippov, G. F. Nuclear Phys., 8, (1958), 237.

65. Davydov, A. S. and Filippov, G. F. JETP, 36, (1959), 1497.

66. Dennison, D. M. Revs. Mod. Phys., 3, (1931), 280.

67. Alburger, D. E. Phys. Rev., 108, (1957), 812.

68. Baggerly, Marmier, Boehm, and DuMond. Phys. Rev., 100, (1955), 1364.

69. Benczer, Farrely, Koerts, and Wu. Phys. Rev., 101, (1955), 1027.

70. Glaubman, M. Phys. Rev., 98, (1955), 645.

71. Jean, M. and Touchard, J. Jour. Phys. Radium, 19, (1958), 56.

72. Arns, Sund, and Wiedenbeck. Phys. Rev., to be published.

73. Peker, L. private communication quoted in Reference 64.

74. Hickman, G. D. Thesis, University of Michigan, 1958.

75. Boehm, Marmier, and DuMond. Phys. Rev., 95, (1954), 864.

76. Lindquist,T. and Marklund, I. Nuclear Phys., 4, (1957), 189.

77. Waddell, R. and Jensen, E. Phys. Rev., 102, (1956), 816.

78. Lide, R. W. Doctoral Thesis, University of Michigan, 1959.

79. Frauenfelder, Levine, Rossi, and Singer. Phys. Rev., 103, (1956), 352.

80. Sund, Arns, and Wiedenbeck. Phys. Rev., to be published.

81. Mraz, J. Nuclear Phys., 4, (1957), 457.

82. Nathan, O. Nuclear Phys., 4, (1957), 125.

83. Ofer, S. Nuclear Phys., 5, (1958), 331.

84. Burson, Jordon, and LeBlanc. Phys. Rev., 94, (1954), 103.

85. Keshishian, Kruse, Klotz, and Fowler. Phys. Rev., 96, (1954), 1050.

86. Bertolini, Bettoni, and Lazzarini. Nuovo Cimento, 3, (1956), 754 Nuovo Cimento, 3, (1956), 1162.

87. Clark, M. A. and Knowles, J. W. Bull. Am. Phys. Soc. Ser. II, 4, (1957), 231.

88. Grigor'ev, Dzhelepov, Zolotavin, Kraft, Kratsik, and Peker. Izv. Akad. Nauk SSSR, Ser. Fiz., 22, (1958) 101.

89. Avotina, Grigor'ev, Zolotavin, and Kratsik. Doklady Akad. Nauk SSSR, 119, (1958), 1127.

90. Bäckstrom, Lindskog, Bergman, Bashandy, and Bäcklin. Arkiv för Fys., 15, (1959), 121.

91. Ewan, Graham, and Geiger. Bull. Am. Phys. Soc. Ser. II, 4, (1959), 292.

92. Ofer, S. and Cohen, S. G. Proc. Rehovath Conf. Nucl. Structure, North-Holland Publishing Co., (Amsterdam, 1958), 479.

93. Haynes, S. K. Phys. Rev., 74, (1948), 423.

94. Mitchell, Zaffarano and Kern. Phys. Rev., 73, (1948), 1424.

95. Bowe, Goldhaber, Hill, Meyerhof, and Sala. Phys. Rev., 73, (1948), 1219.

96. McGowan, F. K. Oak Ridge National Laboratory Report ORNL-952, March, 1951.

97. Kendall, H. W. and Deutsch, M. Massachusetts Institute of Technology Progress Report, February 28, 1955.

98. Bishop, G. R., Wilson, R., and Halban, H. Phys. Rev., 77, (1950), 416.

99. Levkovskii, V. N. Atomnaya Energ., 4, (1958), 79.

100. Johns, M. W., Chidley, B. and Williams, I. R. Phys. Rev., 99, (1955), 1645A.

101. Kraushaar, J. J., Brun, E., Meyerhof, W. E. Phys. Rev., 101, (1956), 139.

102. McGowan, F. K., DeBenedetti, S., Francis, J. E., Jr. Phys. Rev., 75, (1949), 1761.

103. Coleman, C. F. Nuclear Phys., 7, (1958), 488.

104. Brun, E., Kraushaar, J. J. and Meyerhof, W. E. Phys. Rev., 102, (1956), 808.

105. Nuclear Data Sheets, 59-1-25 (National Research Council, Washington, D.C., 1959).

106. Metzger, F. R. Phys. Rev., 101, (1956), 286.

107. Hedgran, A. and Lind, D. Arkiv Fysik, 5, (1952), 177.

108. Goodman, L. S. and Childs, W. J. Bull. Am. Phys. Soc. Ser. II, 3, (1958), 21.

109. Van Patter, D. M. Bull. Am. Phys. Soc. Ser. II, 3, (1958), 212.

110. Temmer, G. M. and Heydenburg, N. P. Phys. Rev., 104, (1956), 967.

111. Scharff-Goldhaber, G. Phys. Rev., 90, (1953), 587.